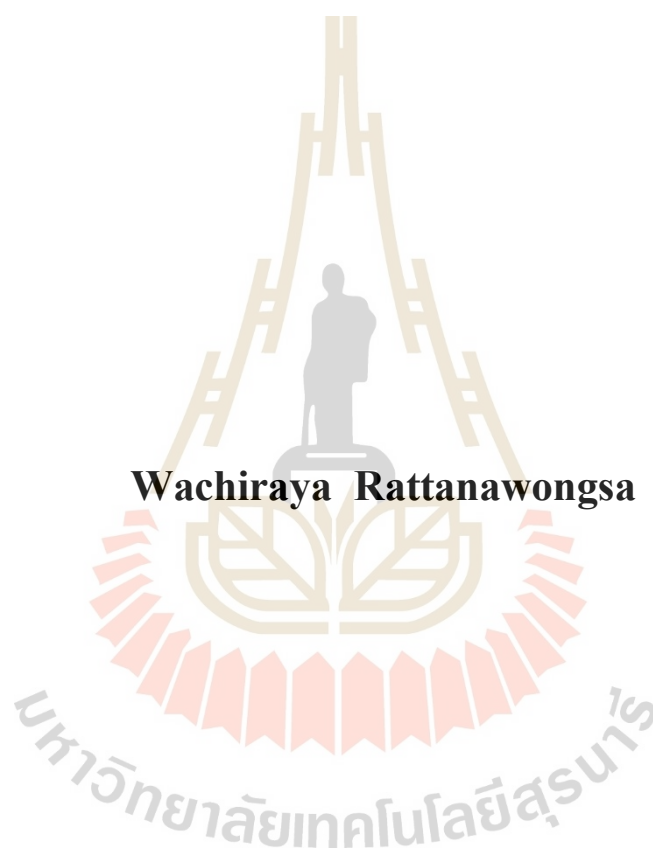


**SYNTHESIS AND CHARACTERIZATION OF CERIUM –  
CONTAINING ZEOLITE Y FROM DIFFERENT  
PREPARATION METHODS**



**Wachiraya Rattanawongsa**

**A Thesis Submitted in Partial Fulfillment of the Requirements for the  
Degree of Master of Science in Chemistry  
Suranaree University of Technology  
Academic Year 2019**

การสังเคราะห์และวิเคราะห์ลักษณะซีไอไลต์ชนิดวาง  
ที่มีการบรรจุของซีเรียมาจากวิธีเตรียมแตกต่างกัน



วิทยานิพนธ์นี้เป็นส่วนหนึ่งของการศึกษาตามหลักสูตรปริญญาวิทยาศาสตรมหาบัณฑิต  
สาขาวิชาเคมี  
มหาวิทยาลัยเทคโนโลยีสุรนารี  
ปีการศึกษา 2562

**SYNTHESIS AND CHARACTERIZATION OF CERIU –  
CONTAINING ZEOLITE Y FROM DIFFERENT  
PREPARATION METHODS**

Suranaree University of Technology has approved this thesis submitted in partial fulfillment of the requirements for the a Master's degree.

Thesis Examining Committee

  
\_\_\_\_\_  
(Prof. Dr. James R. Ketudat-Cairns)

Chairperson

  
\_\_\_\_\_  
(Prof. Dr. Jatuporn Wittayakun)

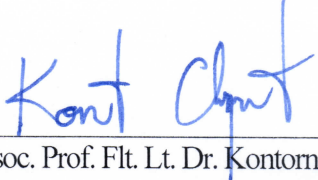
Member (Thesis Advisor)

  
\_\_\_\_\_  
(Assoc. Prof. Dr. Sanchai Prayoonpokarach)

Member

  
\_\_\_\_\_  
(Asst. Prof. Dr. Theeranun Siritanon)

Member

  
\_\_\_\_\_  
(Assoc. Prof. Flt. Lt. Dr. Kontorn Chamniprasart)

Vice Rector for Academic Affairs  
and Internationalization

  
\_\_\_\_\_  
(Assoc. Prof. Dr. Worawat Meevasana)

Dean of Institute of Science

วชิรญาณ รัตนวงษา : การสังเคราะห์และวิเคราะห์ลักษณะซีโอไลต์ชนิดวายที่มีการบรรจุ  
ของซีเรียมจากวิธีเตรียมแตกต่างกัน (SYNTHESIS AND CHARACTERIZATION OF  
CERIUM – CONTAINING ZEOLITE Y FROM DIFFERENT PREPARATION  
METHODS) อาจารย์ที่ปรึกษา : ศาสตราจารย์ ดร.จตุพร วิทยาคุณ, 66 หน้า.

ซีโอไลต์วายที่มีซีเรียม (Ce-NaY) มีการศึกษาและประยุกต์ในหลากหลายปฏิกิริยา  
กระบวนการเติมซีเรียมเข้าไปในซีโอไลต์ส่งผลต่อลักษณะเชิงปฏิกิริยาในทิศทางแตกต่างกัน งานนี้  
สนใจการตรวจสอบรูปแบบกัมมันต์ของ Ce-NaY ที่เตรียมจากวิธีแลกเปลี่ยน ไอออน (Ce-NaY-IE)  
วิธีเอ็บซุ่ม (Ce-NaY-IMP) และวิธีเชื่อม โยง (Ce-NaY-INC) เทคนิคการเลี้ยวเบนของรังสีเอ็กซ์ ฟูล  
เรียร์ทรานส์ฟอรัมสเปกโทรสโกปี และกล้องจุลทรรศน์อิเล็กตรอนแบบส่องกราดเย็นย่น โครงสร้าง  
ฟูจาไซต์ที่มีความเป็นผลึกต่างกัน การเกิดซีเรียมออกไซด์ในทุกตัวอย่างได้จากผลของเทคนิค  
มาน และดีฟิวส์รีแฟลกแทนซ์ ยูวีวิสิเบิลสเปกโทรสโกปี ที่สำคัญ สามารถบอกความแตกต่างของ  
ตำแหน่งกัมมันต์จากการเลือกเกิดผลิตภัณฑ์ของปฏิกิริยาการเปลี่ยนแปลงเมทิลบิวทินอล Ce-NaY-  
IE มีตำแหน่งกรดบรอนสเตด ซึ่งเกิดจากการกำจัดน้ำและการให้ความร้อน ในขณะที่ Ce-NaY-IMP  
มีตำแหน่งเบสจากช่องว่างจากการที่ออกซิเจนในแลตทิซของซีเรียมออกไซด์หายไป Ce-NaY-INC  
มีสมบัติกรด-เบสที่คลุมเครือ ความหลากหลายของตำแหน่งกัมมันต์ในตัวอย่างที่เตรียมด้วยวิธี  
แตกต่างกันจะนำไปสู่ลักษณะเชิงปฏิกิริยาที่ต่างกัน

สาขาวิชาเคมี

ปีการศึกษา 2562

ลายมือชื่อนักศึกษา วชิรญาณ รัตนวงษา

ลายมือชื่ออาจารย์ที่ปรึกษา จตุพร วิทยาคุณ

WACHIRAYA RATTANAWONGSA : SYNTHESIS AND  
CHARACTERIZATION OF CERIUM – CONTAINING ZEOLITE Y FROM  
DIFFERENT PREPARATION METHODS. THESIS ADVISOR : PROF.  
JATUPORN WITTAYAKUN, Ph.D. 66 PP.

CERIUM/ZEOLITE Y/ION EXCHANGE/IMPREGNATION/INCORPORATION

Cerium - containing zeolite Y (Ce-NaY) has been studied and applied in numerous reactions. The introduction strategies of Ce into zeolite influence catalytic activity in different ways. This work focuses on investigating active species of Ce-NaY prepared by ion exchange (Ce-NaY-IE), impregnation (Ce-NaY-IMP) and incorporation (Ce-NaY-INC) methods. The characterization by XRD, FT-IR and SEM reveals the faujasite structure with different crystallinity. The formation of CeO<sub>2</sub> in all samples are deduced from Raman and UV-Vis-DR results. Importantly, active sites of samples are differentiated by products selectivity of methylbutynol (MBOH) transformation reactions. Ce-NaY-IE has Bronsted acid sites produced from the dehydration and heat treatment. While Ce-NaY-IMP has basic sites from the existence of oxygen vacancies within CeO<sub>2</sub> lattice. Ce-NaY-INC has ambiguous acid-base properties. The variety of reactive sites in Ce-NaY samples from different preparation methods could lead to different catalytic activity.

School of Chemistry

Academic Year 2019

Student's Signature วชิรญา รattanawongsa

Advisor's Signature จตุพร Wittayakun

## ACKNOWLEDGEMENTS

I would like to express my deep gratitude to my advisor, Prof.Dr. Jatuporn Wittayakun, for his motivation and encouragement throughout 4 years of my study. I have received many academic advices and experiences from him. In addition, he guided me a lot of meaningful attitudes for learning and living.

I would like to acknowledge Development and Promotion of Science and Technology Talents Project (DPST) scholarship for giving me an opportunity in science studying and Suranaree University of Technology (SUT) for providing workplaces with facilities. I wish to thank all lecturers of School of Chemistry for a warm learning atmosphere that make me be a better and more confident learner. I also thank all staffs for their kind help whenever I have problems with formal documents.

Thank you to all members of Catalysis group for their memorable helps during my time at SUT. I also thank Taylor Swift, my favorite artist. Her sweet songs always heal my mind. In addition, specially thank to my best mate who stays beside me along the way throughout all difficult times.

Last, the grateful thanks are also extended to my parents, my brother and other family members for their unconditional love and support on all situations in my life.

Wachiraya Rattanawongsa

# CONTENTS

	<b>Page</b>
ABSTRACT IN THAI.....	I
ABSTRACT IN ENGLISH .....	II
ACKNOWLEDGEMENTS.....	III
CONTENTS.....	IV
LIST OF TABLES.....	VII
LIST OF FIGURES .....	VIII
<b>CHAPTER</b>	
<b>I INTRODUCTION.....</b>	<b>1</b>
1.1 Introduction.....	1
1.2 References.....	3
<b>II LITERATURE REVIEW .....</b>	<b>5</b>
2.1 Zeolite Y .....	5
2.2 Cerium.....	7
2.3 Cerium-containing zeolite Y and related materials .....	8
2.4 MBOH transformation.....	12
2.5 References.....	15
<b>III EXPERIMENTAL.....</b>	<b>21</b>
3.1 Chemicals.....	21

## CONTENTS (Continued)

	<b>Page</b>
3.2 Preparation of ion Exchange (Ce-NaY-IE) and Impregnation (Ce-NaY-IMP) samples .....	22
3.3 Synthesis of cerium-incorporated sample (Ce-NaY-INC).....	23
3.4 Characterization .....	24
3.4.1 X-ray diffraction (XRD) .....	24
3.4.2 Fourier transform infrared spectroscopy (FTIR) .....	24
3.4.3 Raman spectroscopy .....	24
3.4.4 UV-VIS-DR spectroscopy .....	24
3.4.5 Scanning electron microscopy (SEM) .....	25
3.5 Catalytic activity testing by transformation of MBOH.....	25
3.6 References.....	27
<b>IV RESULTS AND DISCUSSION .....</b>	<b>29</b>
4.1 Phase analysis by X-ray diffraction .....	29
4.2 Functional groups and forms of Ce species by spectroscopy .....	31
4.2.1 Fourier transform infrared spectroscopy .....	31
4.2.2 Raman spectroscopy .....	33
4.2.3 UV-VIS Diffuse Reflectance Spectroscopy .....	35
4.3 Morphology observation by scanning electron microscopy .....	37
4.4 Catalytic transformation of methylbutynol (MBOH) .....	40
4.5 References.....	47

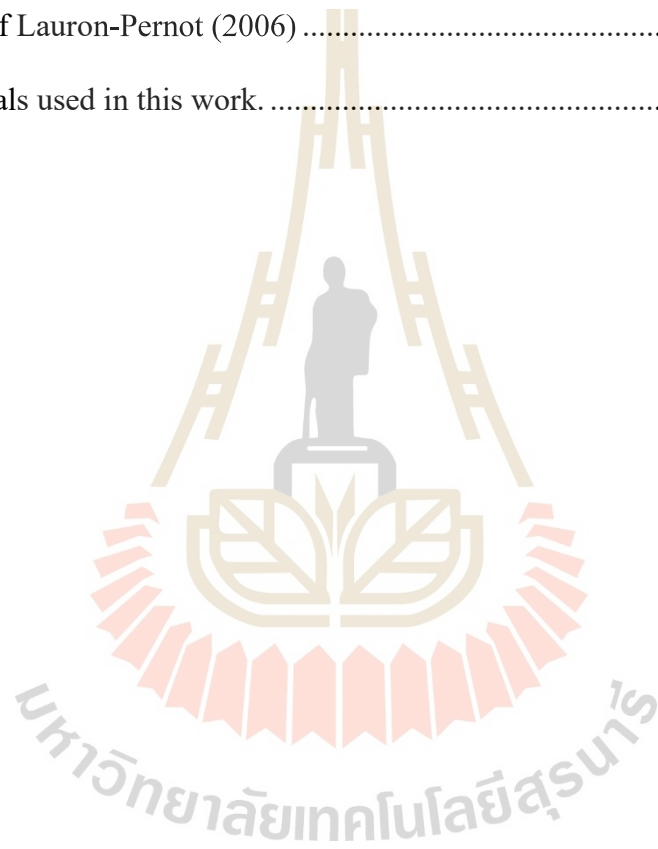
**CONTENTS (Continued)**

	<b>Page</b>
<b>V CONCLUSION .....</b>	<b>53</b>
<b>APPENDIX.....</b>	<b>54</b>
<b>CURRICULUM VITAE.....</b>	<b>66</b>



## LIST OF TABLES

Table	Page
2.1 Some previous works of activity testing by MBOH conversion from review article of Lauron-Pernot (2006) .....	14
3.1 Chemicals used in this work. ....	21

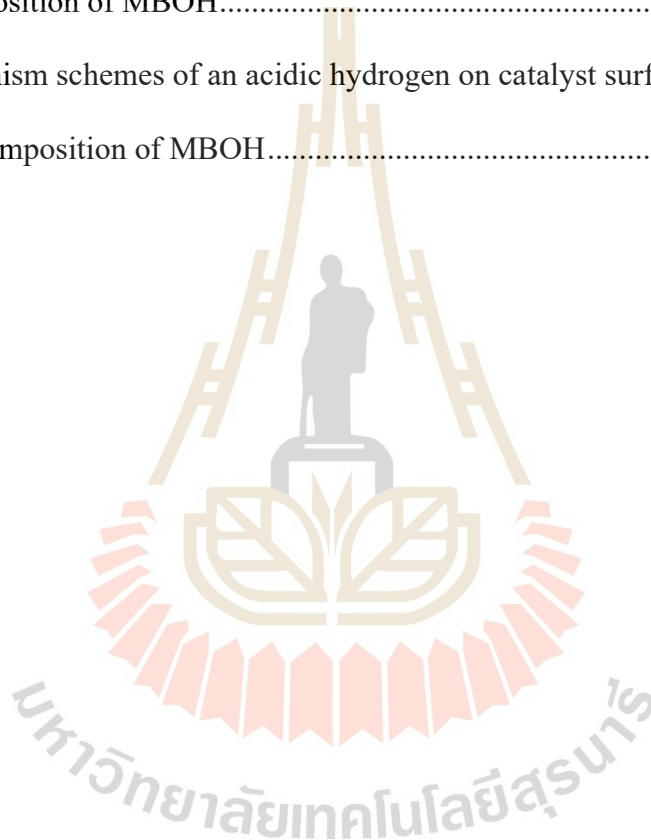


## LIST OF FIGURES

Figure	Page
2.1 Primary Building Unit (PBU) and the linkage with another unit of zeolite (a), FAU framework formation by the connection of <i>sod</i> cages and D6Rs (b), and 3D framework of FAU with pore identification.....	6
2.2 Cation sites in FAU.....	7
2.3 Mechanism model for migration process of Ce(III) .....	9
2.4 Reaction scheme of MBOH conversion over different active sites of a catalyst.....	13
3.1 Operation apparatus.....	27
4.1 XRD patterns of NaY, Ce-NaY-IE, Ce-NaY-IMP and Ce-NaY-INC.....	30
4.2 FTIR spectra of NaY, Ce-NaY-IE, Ce-NaY-IMP and Ce-NaY-INC.....	33
4.3 Raman spectra of NaY, Ce-NaY-IE, Ce-NaY-IMP, Ce-NaY-INC and CeO <sub>2</sub> .....	34
4.4 UV-DR spectra of CeO <sub>2</sub> , Ce-NaY-IE, Ce-NaY-IMP and Ce-NaY-INC with the powder color of modified NaY samples.....	36
4.5 SEM micrographs of NaY (a) - (c), Ce-NaY-IE (d) - (f), Ce-NaY-IMP (g) - (i) and Ce-NaY-INC (j) -(l). .....	39
4.6 MBOH conversion of NaY, Ce-NaY-IE, Ce-NaY-IMP and Ce-NaY-INC.....	40
4.7 Products selectivity from MBOH conversion of NaY, Ce-NaY-IE, Ce-NaY-IMP and Ce-NaY-INC samples.....	41

**LIST OF FIGURES (Continued)**

<b>Figure</b>	<b>Page</b>
4.8 The color of catalyst powder before and after reaction testing.....	45
4.9 Mechanism schemes of Lewis acid-base pair catalyze the decomposition of MBOH.....	45
4.10 Mechanism schemes of an acidic hydrogen on catalyst surface catalyze the decomposition of MBOH.....	46



# CHAPTER I

## INTRODUCTION

### 1.1 Introduction

Cerium - containing zeolite Y has been prepared from various strategies for applying in numerous reactions. The Ce introduction methods influence final Ce forms and material properties that produce the different functions of heterogenous catalyst. Many researchers have been studying the catalytic properties of Ce - containing zeolite Y from various preparation methods. For instance, Fillipe et al. (2011); Du et al. (2013); Sousa-Aguiar et al. (2013); Li et al. (2015); Roth et al. (2016) investigated the introduction of Ce in zeolite Y by ion exchange with initial cations of zeolite (normally  $\text{Na}^+$  or  $\text{NH}_4^+$ ). The process provides acid sites for material. In addition, Ce-exchanged zeolite Y could produce  $\text{CeO}_2$  species (Zu et al., 2019) which itself contains basic property. That useful for the reactions of required-basic sites (Atwood, 2012). Apart from that, an impregnation method could distribute  $\text{CeO}_2$  phase on zeolite as reported by Haung et al. (2010) Schelter (2013); Aneggi et al. (2016). Besides the mentioned of post modification between Ce and zeolite, there is an incorporation method of in situ adding Ce precursor during the zeolite synthesis (Xie et al., 2017). The works of Wu et al. (2010); Roth et al. (2016) and Li et al. (2019) revealed that inserting cerium into the framework position of MCM-22 and mordenite zeolite can provoke acidity

Taking into account that different methods of introduction Ce into zeolite Y produce material properties in different ways. Mohamed et al. (2005) proposed the assumption that Ce are highly sensitive towards preparation methods. These points lead to a question of what is an active site of the material which contains zeolite Y and Ce prepared from different strategies, in terms of acid-base catalytic property. At last, this curiosity turns into a main focus of this work.

Herein, the preparation and characterization of Ce-containing zeolite Y from 3 different processes including ion exchange, impregnation and incorporation are involved in this work. The first and second methods are carried out through commercial zeolite Y as parent material. Meanwhile, for incorporation, Ce precursor is added simultaneously along during zeolite synthesis. All samples are characterized by various techniques comprising XRD, FT-IR, Raman, DR-UV spectroscopy and SEM and discussed regarding the obtained phases, the possible species and location of Ce together with the effect of preparation strategies to zeolite structure and morphology. The characteristics of parent zeolite Y is compared in all techniques.

Besides, the attentiveness of this work is clarifying the catalytic activity in terms of acidity and basicity of the material. Hence, a reaction testing of the 2-methylbut-3-yn-2-ol (MBOH) transformation is demonstrated. The conversion and product selectivity from tested reaction are considered to differentiate a catalyst property. The results showed that Ce-containing samples provided different catalytic activity. Therefore, the active sites of all samples are explained by a variety of products from MBOH transformation. Furthermore, the acid-base property is discussed in relation to obtained phases from characterization analysis.

## 1.2 References

- Atwood, D. A. (Editor). (2012) *The Rare Earth Elements: Fundamentals and Applications*. **John Wiley & Sons Ltd, West Sussex**.
- Aneggi, E., Boaro, M., Colussi, S., de Leitenburg, C. and Trovarelli, A. (2016). Chapter 289 - Ceria-Based Materials in Catalysis: Historical Perspective and Future Trends. In J.-C. G. Bünzli and V. K. Pecharsky (Eds.) *Handbook on the Physics and Chemistry of Rare Earths* 50: 209-242: **Elsevier B.V., Amsterdam**.
- Du, X., Gao, X., Zhang, H., Li, X. and Liu, P. (2013). Effect of cation location on the hydrothermal stability of rare earth-exchanged Y zeolites. **Catalysis Communications**. 35: 17-22.
- Huang, Q., Xue, X. and Zhou, R. (2010). Decomposition of 1,2-dichloroethane over CeO<sub>2</sub> modified USY zeolite catalysts: Effect of acidity and redox property on the catalytic behavior. **Journal of Hazardous Materials**. 183(1): 694-700.
- Li, Y., Huang, S., Cheng, Z., Cai, K., Li, L., Milan, E., Lv, J., L., Wang, Y., Sun, Q. and Ma, X. (2019). Promoting the activity of Ce-incorporated MOR in dimethyl ether carbonylation through tailoring the distribution of Brønsted acids. **Applied Catalysis B: Environmental**. 256, art. 117777.
- Mohamed, M. M., Salama, T. M., Othman, A. I. and El-Shobaky, G. A. (2005). Low temperature water-gas shift reaction on cerium containing mordenites prepared by different methods. **Applied Catalysis A: General**. 279(1): 23-33.
- Roth, W. J., Gil, B., Makowski, W., Sławek, A., Korzeniowska, A., Grzybek, J., Siwek, M. and Michorczyk, P. (2016). Framework-substituted cerium MCM-

22 zeolite and its interlayer expanded derivative MWW-IEZ. **Catalysis Science & Technology**. 6(8): 2742-2753.

Schelter, E. J. (2013). Cerium under the lens. **Nature Chemistry**. 5: 348.

Sousa-Aguiar, E. F., Trigueiro, F. E. and Zotin, F. M. Z. (2013). The role of rare earth elements in zeolites and cracking catalysts. **Catalysis Today**. 218-219: 115-122.

Wu, Y., Wang, J., Liu, P., Zhang, W., Gu, J. and Wang, X. (2010). Framework-Substituted Lanthanide MCM-22 Zeolite: Synthesis and Characterization. **Journal of the American Chemical Society**. 13: 17989-17991.

Xie, J., Zhuang, W., Yan, N., Du, Y., Xi, S., Zhang, W., Tang, J., Zhou, Y. and Wang, J. (2017). Directly synthesized V-containing BEA zeolite: Acid-oxidation bifunctional catalyst enhancing C-alkylation selectivity in liquid-phase methylation of phenol. **Chemical Engineering Journal**. 328: 1031-1042.

Zu, Y., Hui, Y., Qin, Y., Zhang, L., Liu, H., Zhang, X., Guo, Z., Song, L. and Gao, X. (2019). Facile fabrication of effective Cerium (III) hydroxylated species as adsorption active sites in CeY zeolite adsorbents towards ultra-deep desulfurization. **Chemical Engineering Journal**. 375, art. 122014.

## CHAPTER II

### LITERATURE REVIEW

#### 2.1 Zeolite Y

Zeolite is crystalline microporous aluminosilicate with well-defined cavities and/or channels. It is constructed from  $[\text{SiO}_4]$  and  $[\text{AlO}_4]^-$  or Primary Building Units (PBUs) that are linked by sharing corner oxygen atom (Figure 2.1(a)). The Al-containing in tetrahedron PBU, results in the net negative charge in the structure, which requires charge balancing cations (normally  $\text{Na}^+$ ) from Si and/or Al precursors.

Zeolite Y has the 3D framework of a faujasite (FAU) structure from PBUs as double 6-rings (D6Rs) and sodalite (*sod*) cages (Figure 2.1(b)). Then, each *sod* cage connects with four D6Rs, while each D6Rs links to two *sod* cages, resulting in a 3D channel framework with 12-ring pore openings that are called supercage with pore size dimension of 1.3 nm. FAU is in a cubic crystal system with  $a = 24.74 \text{ \AA}$  (Figure 2.1(c)). FAU structure is divided into 2 types including zeolite X and Y depending on Si and Al content. As the unit cell of hydrated FAU is  $[\text{M}_a (\text{H}_2\text{O})_b][\text{Al}_a\text{Si}_{192-a}\text{O}_{384}]$ , where  $a$  is Al atom numbers per unit cell and M is monovalent cation (or one-half of a divalent cation). Since this work focus on Y type, the value “ $a$ ” can vary less than 76 Al atoms that corresponds to Si/Al ratios of zeolite is higher than 1.5 (Kulprathipanja, 2010).

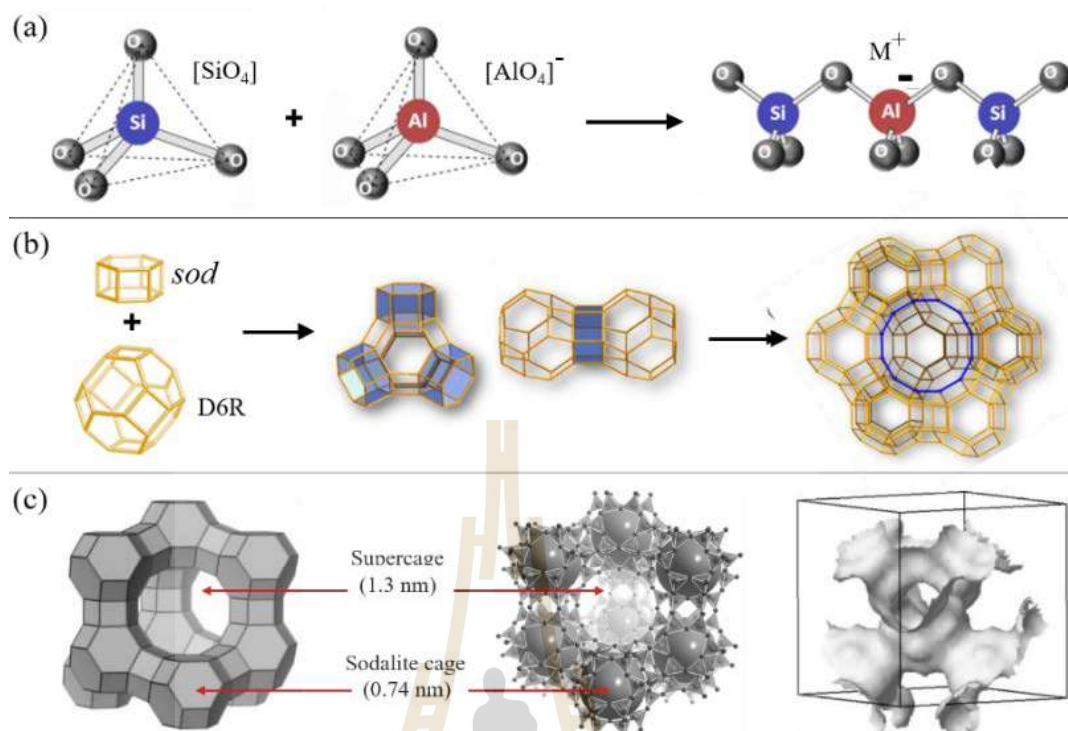


**Figure 2.1** Primary Building Unit (PBU) and the linkage with another unit of zeolite (a), FAU framework formation by the connection of *sod* cages and D6Rs (b), and 3D framework of FAU with pore identification (adapted from Kulprathipanja, 2010; Guo, 2016).

The distribution of cation sites (this case is  $\text{Na}^+$ ) of FAU has been reported by Frising and Leflaive (2008). As shown in Figure 2.2,  $\text{Na}^+$  cations tend to occupy sites which maximize the interaction with framework oxygen atoms and minimize cation-cation electrostatic repulsion. The cations could be exchanged with other types of cation. Then, the distributions among the sites are different from the sodium form because of the differences in cation size and charge. The changes of non-framework cations could modify the zeolite properties.

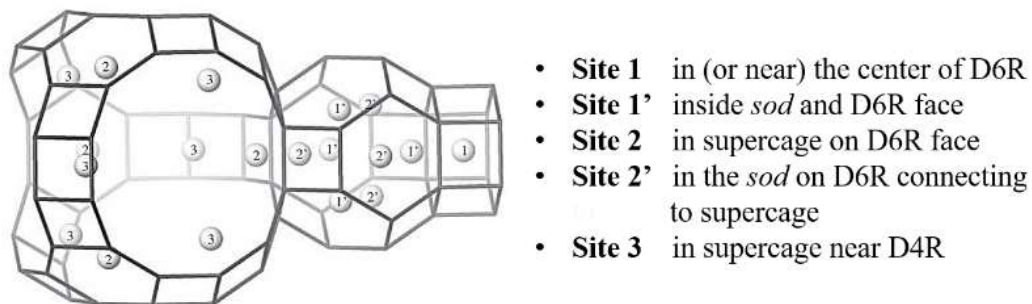


**Figure 2.2** Cation sites in FAU (Kulprathipanja, 2010).

## 2.2 Cerium

Cerium (Ce,  $Z=58$ ) is an element in lanthanide series. It is the most abundant rare-earth metal and it is not really rare because it ranks as the 26<sup>th</sup> of most abundant element on the earth's crust (Dahle and Arai, 2015). Its electronic configuration is  $[\text{Xe}] 4f^1 5d^1 6s^2$ . Ce commonly exists as trivalent *Cerous* state ( $\text{Ce}^{3+}$ ) and tetravalent *Ceric* state ( $\text{Ce}^{4+}$ ) which has unique stability attributed to empty 4f-shell electronic configuration. Most of other lanthanides are stable in trivalent state. In addition, Ce can form various kinds of materials because its coordination numbers are between 3 and 12 but the most common coordination number is 8. This is superior to transition metals owing to its larger ionic radius (Huang, 2010). Ce is used in various applications, including structural metal alloys, polishing, self-cleaning ovens, automotive catalytic converters, phosphors and pigment stabilization, solid-oxide fuel cells, electronic applications, magnets, and catalysts (King et al., 2016).

### 2.3 Cerium-containing zeolite Y and related materials

Corma and Lopez Nieto. (2000) gathered the information of “the use of rare-earth-containing zeolite catalyst” published on *Handbook on the Physics and Chemistry of Rare Earths: Chapter 185*. They explained that, usually, the introduction of cerium into zeolite Y can be achieved by solution or solid-state ion exchange of the sodium or ammonium forms of zeolites. A trivalent cation of cerium replaces 3 monovalent cations in the exchangeable positions within the supercage. The Ce-exchanged zeolite is defined as acid material. For instances, Fillipe et al. (2011); Du et al. (2013) and Li et al. (2015) reported acidity of Ce-containing zeolite Y from aqueous impregnation with Ultra Stable Y (USY) zeolite with  $\text{NH}_4^+$  form, double-exchange double-calcination (DEDC) and ion exchange in aqueous with  $\text{Na}^+$  form, respectively. In addition, that acid property could be obtained in the preparation from different strategies. As far the process undergoes through liquid media of Ce ions and zeolite powder at temperature higher than  $25^\circ\text{C}$  (the selected work is operated at  $80\text{--}90^\circ\text{C}$ ) for a certain period of time and followed by calcination of oxide transformation temperature. Fillipe et al. (2011) defined the species of Ce from FT-Raman spectra in term of  $\text{CeO}_2$ , similarly, as the works of Lee et al. (2019); Zu et al. (2019). While Du et al. (2013) and Li et al. (2015) observed  $\text{Ce}_2\text{O}_3$  and  $\text{CeO}_2$  or both  $\text{Ce}^{3+}$  and  $\text{Ce}^{4+}$  from XPS analysis.

In case of Ce location, Du et al. (2013) and Li et al. (2015) described similarly. As initially,  $\text{Ce}(\text{H}_2\text{O})_n^{3+}$  located in supercages (Figure 2.3). During thermal treatment,  $\text{Ce}(\text{OH})^{2+}$  is formed via dehydration. Then calcination provides  $\text{CeO}_2$  formation, simultaneously, it gives driving force for some  $\text{Ce}(\text{OH})^{2+}$  to migrates and locate in sodalite cage.

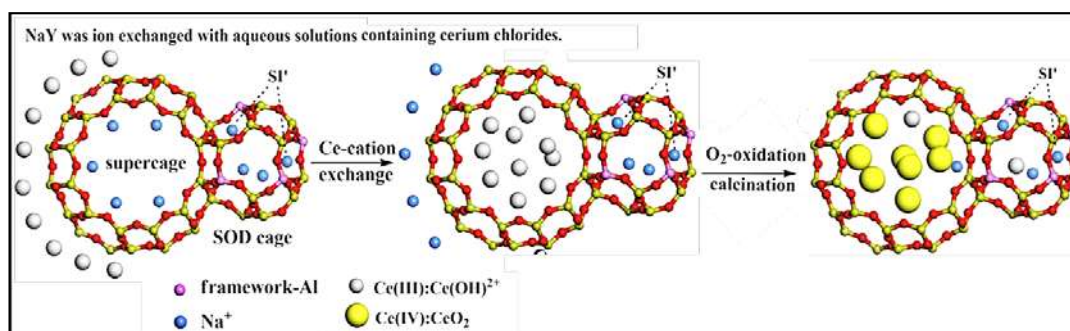


**Figure 2.3** Mechanism model for migration process of Ce(III) (adapted from Li et al., 2015).

In addition, the mentioned process explains the acidity of catalyst that supports pyridine adsorption results of Fillipe et al. (2011) and Li et al. (2015). As the partial hydrolysis of hydrated Ce or rare-earth ions produce H<sup>+</sup>, as shown in the following equations (Falabella et al., 2013) that attributes the formation of Bronsted acid sites through bridged hydroxyls (Du et al., 2013).



In addition to ion exchange, there is the impregnation method that has been used for introducing Ce into zeolite Y (Krishna Reddy et al., 2009; Huang et al., 2010; Saceda et al., 2012; Cheng et al., 2019). The main objective of this method is zeolite Y is to be used as a porous support for improving the dispersion of Ce and/or stabilizing the catalyst by the interaction between support and active species (Perego and Villa, 1997). The active Ce form is cerium oxide (CeO<sub>2</sub>), since the material is normally calcined after impregnated. From my understanding, this material is regularly used as a redox catalyst rather than as base catalyst because CeO<sub>2</sub> has been

known as an oxygen storage from unique ability of reversible valence between  $\text{Ce}^{4+}$  in  $\text{CeO}_2$  and  $\text{Ce}^{3+}$  in  $\text{Ce}_2\text{O}_3$  (Saceda et al., 2012).

Generally, solid surfaces simultaneously provide both acid and basic sites (Cutrufello et al., 2002). In case of  $\text{CeO}_2$ , surface  $\text{Ce}^{4+}$  and  $\text{OH}^{\delta+}$  species are the main sources of acidity while basic property is related to surface  $\text{O}^{2-}$  and hydroxyl groups ( $\text{OH}^{\delta-}$ ). The  $\text{CeO}_2$  is basicity-dominated catalyst due to oxygen vacancies also contribute to Lewis basic sites by producing 2 unpaired electrons (Chen et al., 2017). Hence, the basicity is used in various reactions i.e. oxidative coupling of methane (OCM) to C2 products (ethylene/ethane) and transesterification of triglycerides to glycerol and fatty acid methyl esters (FAME) (Atwood, 2012).

In addition, the basic property is useful as the places for acid reactants attacking. As Mohamed et al. (2005) stated that CO gases responded to  $\text{CeO}_2$  of Ce-containing mordenite zeolite for further catalytic process of water-gas shift reaction. In a similar way, the prepared  $\text{CeO}_2$ -comprising zeolite by impregnation displayed the co-operation performance. For more instances, Zhou et al. (2008) and Huang et al. (2010) found the synergy between  $\text{CeO}_2$  species and USY zeolite improves the catalytic activity of the 1,2-dichloroethane (DCE) oxidation reaction by strong adsorption of DCE. That resulted in high selectivity of the products ( $\text{HCl}$ ,  $\text{CO}_2$  and  $\text{Cl}_2$ ) which evaluated by micro-reaction testing. Moreover, Saceda et al. (2012) remarked that acidic sites of zeolite Y is available positions for reactant adsorption of ethanol oxidation. That mean it was easy for  $\text{CeO}_2$  to convert  $\text{C}_2\text{H}_5\text{OH}$  to  $\text{CO}_2$  and  $\text{H}_2\text{O}$ .

Apart from above methods of adding Ce, there is a method that Ce salt is added simultaneously with zeolite precursors (Laha et al., 2002). From Mohamed et

al. (2005), they reported that incorporation of cerium during the synthesis of mordenite zeolite is believed to serve as catalytic sites differing from via post-synthesis such as ion exchange or impregnation. Since, Ce is incorporated presumably into the framework position or called isomorphous substitution which also prevent the leaching of active species (Liu et al., 2017).

However, from my best knowledge, incorporation of Ce into zeolite Y or FAU framework has not been reported. This might due to size incompatibility between Ce and Al and/or Si ions (Laha et al., 2002). Nevertheless, various type of zeolites and related materials have been synthesized from this strategy, for examples, Ce in the framework of siliceous mesopore MCM-41 by Laha et al. (2002); Ce<sup>4+</sup> framework-incorporated MOR and ZSM-5 zeolite from Salama et al. (2005); framework-substituted of lanthanides (La and Ce) in MCM-22 zeolite by Wu et al. (2010); cerium incorporated in MCM-22 zeolite by Roth et al. (2016). Most of mentioned work investigated Ce species by UV-Vis-DR spectroscopy. In addition, temperature programmed desorption of NH<sub>3</sub> (NH<sub>3</sub>-TPD) and FTIR spectroscopy based on pyridine adsorption are used to study the acid-base properties.

The Ce species are highly sensitive towards preparation methods (Mohamed et al., 2005), To understand the different behavior of cerium-containing zeolites prepared by different strategies, it is necessary to know the nature and location of the cerium species in the catalyst (Moreira et al., 2007). Besides conventional characterization; spectroscopic techniques (FTIR, Raman, Uv-Vis, XPS, NMR); microscopic methods (SEM, TEM); temperature program analysis (CO, NH<sub>3</sub>-desorption), a catalytic reaction testing is one alternative tool for studying material actions.

## 2.4 MBOH transformation

Apart from referred methods, catalytic reaction tests are also studied as characterization method for activity surface of inorganic solids (Lauron-Pernot et al., 1991). The properties of the solid are revealed by the catalytic behavior of the reactive probe molecule. Lauron-Pernot (2006) listed the advantages of this method. It is only sensitive to active sites of a solid catalyst, whereas a nonreactive probe molecule can be adsorbed on nonactive sites. The reaction is detected even small number of sites hence it is easy to adjust the operating conditions (temperature, flow rate, weight of catalyst). Finally, the probe molecule is able to give different products produced by different sites on catalyst surface

Herein, 2-methylbut-3-yn-2-ol (MBOH), the simplest tertiary alkynol, is a versatile and readily available chemicals therefore it is selected as diagnostic tool or probe molecule in this work. Since, MBOH is usually transformed into various products when reacts on acidic, basic or coordinatively unsaturated (defect) sites as depicted in Figure 2.4.

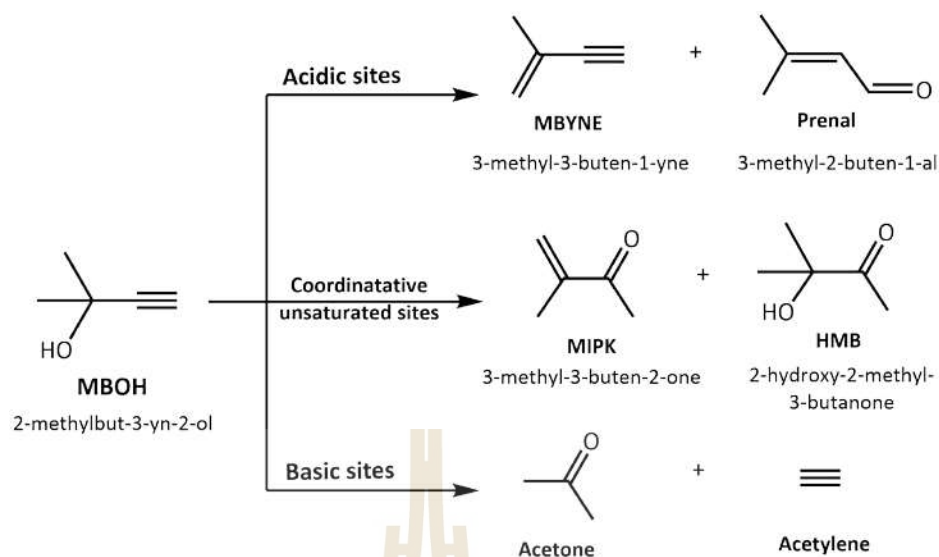


**Figure 2.4** Reaction scheme of MBOH conversion over different active sites of a catalyst (Novikova et al., 2014).

Many researchers have applied MBOH conversion for unambiguous differentiation between acidic, basic and amphoteric surface sites of various materials since 1991 (Table 2.1). In addition, AlSawalha and Roessner (2008) stated that it is a powerful test reaction that clearly defines acid and basic sites from products, however, the amphoteric sites are perhaps difficult to understand. Later on, it was suggested to substitute the term “amphoteric sites” by the “coordinatively unsaturated sites”.

**Table 2.1** Some previous works of activity testing by MBOH conversion from review article of Lauron-Pernot (2006).

	<b>Material</b>	<b>Catalyst weight (g)</b>	<b>Temperature (°C)</b>	<b>Reported properties</b>	<b>Authors</b>	<b>Year</b>
Inorganic oxides	Silica, alumina, zirconia, magnesia	0.4000	180	A and B	Lauron-Pernotd	1991
	Zinc and magnesium oxides and aluminates	0.0125	180	B	Lavalley	1994
	Zirconia	0.020	180	AMPH	Lavalley	1997
	Cs <sup>+</sup> , Ba <sup>2+</sup> , Y <sup>3+</sup> modified MgO catalysts	0.250	70	B	KnÖ-zinger	1999, 2000
	MgO	0.020	120	B	Lauron-Pernotd	2005
Zeolites	Alkali-exchanged	0.050	180	A and B	Kalia-guine	1993
	Alkali-exchanged	3	120	B	Hoel-derich	1999

Notation: A = acidity, B = basicity, and AMPH = amphoteric character.

Interpretation from MBOH reaction test, for instance, Supamathanon et al., 2012 studied catalytic properties of potassium oxide supported on zeolite NaY (K/NaY). They prepared the catalysts from impregnation method by using a mixture of  $\text{CH}_3\text{COOK}/\text{CH}_3\text{COOH}$  to give potassium loadings of 4, 8 and 12 wt%. They found that increasing potassium resulting in significant higher conversion of MBOH than that of pure NaY. That mean introducing K species could improve catalytic performance.

In addition, the products selectivity over time on stream of all materials is crucial results for defining the reactivity sites. The acetone, acetylene and MBYNE are detected as main products of NaY. Herein, the authors concluded that the surface of NaY contained predominantly basic sites and a moderate number of acidic sites. In case of the K/NaY samples, acetone and acetylene are the major products. So, the authors indicated that impregnation with potassium suppressed the acidic sites of NaY. Moreover, Meyer and Hoelderich (1993) already summarized that the basic sites were generated in the zeolite NaX after loading alkali metal cations and alkaline metal oxides by ion exchange (aqueous solution of cesium acetate) and the impregnation (methanolic solution of sodium azide) method, respectively.

## 2.5 References

AlSawalha, M. and Rößner, F. (2008). Characterization of surface properties of silica alumina by catalytic conversion of methylbutynol. **Сорбционные и хроматографические процессы**. 8(2): 192-201.

- Chen, W., Ran, R., Weng, D., Wu, X., Zhong, J. and Han, S. (2017). Influence of morphology on basicity of CeO<sub>2</sub> and its use in 2-chloroethyl ethyl sulfide degradation. **Journal of Rare Earths**. 35(10): 970-976.
- Cheng, X., Huang, L., Yang, X., Elzatahry, A. A., Alghamdi, A. and Deng, Y. (2019). Rational design of a stable peroxidase mimic for colorimetric detection of H<sub>2</sub>O<sub>2</sub> and glucose: A synergistic CeO<sub>2</sub>/Zeolite Y nanocomposite. **Journal of Colloid and Interface Science**. 535: 425-435.
- Corma, A. and Lopez Nieto, J. M. (2000). Chapter 185 The use of rare-earth-containing zeolite catalyst. Gschneidner, K.A. and Eyring, L. (Eds.) Handbook on the Physics and Chemistry of Rare Earths. 29: 269-313. **Elsevier Science B.V., Amsterdam**.
- Cutrufello, M. G., Ferino, I., Monaci, R., Rombi, E. and Solinas, V. (2002). Acid-Base Properties of Zirconium, Cerium and Lanthanum Oxides by Calorimetric and Catalytic Investigation. **Topics in Catalysis**. 19(3): 225-240.
- Dahle, J. T. and Arai, Y. (2015). Environmental geochemistry of cerium: applications and toxicology of cerium oxide nanoparticles. **International Journal of Environmental Research and Public Health**. 12: 1253-1278.
- Du, X., Gao, X., Zhang, H., Li, X. and Liu, P. (2013). Effect of cation location on the hydrothermal stability of rare earth-exchanged Y zeolites. **Catalysis Communications**. 35: 17-22.
- Falabella, E., Trigueiro, F. and Zotin, F. (2013). The role of rare earth elements in zeolites and cracking catalysts. **Catalysis Today**. 218-219: 115-122.
- Fillipe A. C, G., Araújo, D. R., Silva, J. C. M., Macedo, J. L. d., Ghesti, G. F., Dias, S. C. L., Dias, José A. and R.Filho, G. N. (2011). Effect of cerium loading on

- structure and morphology of modified Ce-USY zeolites. **Journal of the Brazilian Chemical Society**. 22: 1894-1902.
- Frising, T. and Leflaive, P. (2008). Extraframework cation distributions in X and Y faujasite zeolites: a review, **Microporous Mesoporous Material**. 114: 27 – 63.
- Guo, P. (2016). Structure determination and prediction of zeolites-- a combined study by electron diffraction, powder X-ray diffraction and database mining. **Doctoral Thesis**. Department of Materials and Environmental Chemistry Arrhenius Laboratory, Stockholm University.
- Huang, Q., Xue, X. and Zhou, R. (2010). Decomposition of 1,2-dichloroethane over CeO<sub>2</sub> modified USY zeolite catalysts: Effect of acidity and redox property on the catalytic behavior. **Journal of Hazardous Materials**. 183(1): 694-700.
- King, A. H., Eggert, R. G. and Gschneidner, K. A. (2016). Chapter 283 The rare earths as critical materials. **Handbook on the Physics and Chemistry of Rare Earths**. 50: 19-46.
- Krishna Reddy, J., Suresh, G., Hymavathi, C. H., Durga Kumari, V. and Subrahmanyam, M. (2009). Ce (III) species supported zeolites as novel photocatalysts for hydrogen production from water. **Catalysis Today**. 141(1): 89-93.
- Kulprathipanja, S. (2010). Zeolite in industrial separation and catalysis. **Weinheim, Wiley-VCH Verlag GmbH & Co. KGaA**.
- Laha, S. C., Mukherjee, P., Sainkar, S. R. and Kumar, R. (2002). Cerium containing MCM-41-type mesoporous materials and their acidic and redox catalytic properties. **Journal of Catalysis**. 207: 213-223.

- Lauron-Pernot, H., Luck, F. and Popa, J. M. (1991). Methylbutynol: a new and simple diagnostic tool for acidic and basic sites of solids. **Applied Catalysis**. 78(2): 213-225.
- Lauron-Pernot, H. (2006). Evaluation of surface acido-basic properties of inorganic-based solids by model catalytic alcohol reaction networks. **Catalysis Reviews**. 48(3): 315-361.
- Lee, K. X., Wang, H., Karakalos, S., Tsilomelekis, G. and Valla, J. A. (2019). Adsorptive desulfurization of 4,6-dimethyldibenzothiophene on bimetallic mesoporous Y zeolites: effects of Cu and Ce composition and configuration. **Industrial and Engineering Chemistry Research**. 58(39): 18301-18312.
- Li, J., Zeng, P., Zhao, L., Ren, S., Guo, Q., Zhao, H., Wang, B., Liu, H., Pang, X., Gao, X. and Shen, B. (2015). Tuning of acidity in CeY catalytic cracking catalysts by controlling the migration of Ce in the ion exchange step through valence changes. **Journal of Catalysis**. 329: 441-448.
- Liu, X., Zhong, S., Yang, F., Su, H., Lin, W., Chen, J., Peng, L., Zhou, S. and Kong, Y. (2017). Template-free synthesis of high-content vanadium-doped ZSM-5 with enhanced catalytic performance. **Chemistry Select**. 2: 11513-11520.
- Meyer, U. and Hoelderich, W. F. (1999). Application of basic zeolites in the decomposition reaction of 2-methyl-3-butyn-2-ol and the isomerization of 3-carene. **Journal of Molecular Catalysis A: Chemical**. 142(2): 213-222.
- Mohamed, M. M., Salama, T. M., Othman, A. I. and El-Shobaky, G. A. (2005). Low temperature water-gas shift reaction on cerium containing mordenites prepared by different methods. **Applied Catalysis A: General**. 279(1): 23-33.

- Moreira, C. R., Pereira, M. M., Alcobé, X., Homs, N., Llorca, J., Fierro, J. L. G. and Ramírez de la Piscina, P. (2007). Nature and location of cerium in Ce-loaded Y zeolites as revealed by HRTEM and spectroscopic techniques. **Microporous and Mesoporous Materials**. 100(1): 276-286.
- Novikova, L., Roessner, F., Belchinskaya, L., AlSawalha, M. and Krupskaya, V. (2014). Study of surface acid–base properties of natural clays and zeolites by the conversion of 2-methylbut-3-yn-2-ol. **Applied Clay Science**. 101: 229-236.
- Perego, C. and Villa, P. (1997). Catalyst preparation methods. **Catalysis Today**. 34(3): 281-305.
- Roth, W. J., Gil, B., Makowski, W., Sławek, A., Korzeniowska, A., Grzybek, J., Siwek, M. and Michorczyk, P. (2016). Framework-substituted cerium MCM-22 zeolite and its interlayer expanded derivative MWW-IEZ. **Catalysis Science & Technology**. 6(8): 2742-2753.
- Saceda, J.-J. F., Rintramee, K., Khabuanchalad, S., Prayoonpokarach, S., de Leon, R. L. and Wittayakun, J. (2012). Properties of zeolite Y in various forms and utilization as catalysts or supports for cerium oxide in ethanol oxidation. **Journal of Industrial and Engineering Chemistry**. 18(1): 420-424.
- Salama, T. M., Mohamed, M. M., A, I. O. and El-Shobaky, G. A. (2005). Structural and textural characteristics of Ce-containing mordenite and ZSM-5 solids and FT-IR spectroscopic investigation of the reactivity of NO gas adsorbed on them. **Applied Catalysis A: General**. 286(1): 85-95.
- Supamathanon, N., Supronowicz, W., Roessner, F., Wittayakun, J. and Prayoonpokarach, S. (2012). Basic properties of potassium oxide supported on

zeolite Y studied by pyrrole-TPD and catalytic conversion of methylbutynol.

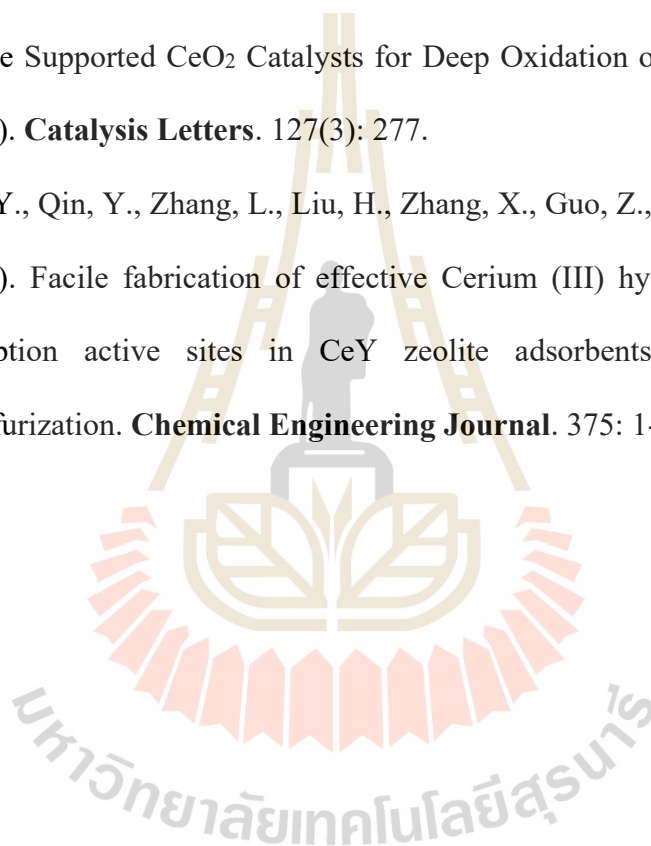
**Química Nova.** 35(9): 1719-1723.

Wu, Y., Wang, J., Liu, P., Zhang, W., Gu, J. and Wang, X. (2010). Framework-Substituted Lanthanide MCM-22 Zeolite: Synthesis and Characterization.

**Journal of the American Chemical Society.** 13: 17989-17991.

Zhou, J., Zhao, L., Huang, Q., Zhou, R. and Li, X. (2008). Catalytic Activity of Y Zeolite Supported CeO<sub>2</sub> Catalysts for Deep Oxidation of 1, 2-Dichloroethane (DCE). **Catalysis Letters.** 127(3): 277.

Zu, Y., Hui, Y., Qin, Y., Zhang, L., Liu, H., Zhang, X., Guo, Z., Song, L. and Gao, X. (2019). Facile fabrication of effective Cerium (III) hydroxylated species as adsorption active sites in CeY zeolite adsorbents towards ultra-deep desulfurization. **Chemical Engineering Journal.** 375: 1-12.



## CHAPTER III

### EXPERIMENTAL

#### 3.1 Chemicals

Chemicals used in this work are listed in Table 3.1

**Table 3.1** Chemicals used in this work.

Chemicals	Formula	Content	Supplier
Tetraethyl orthosilicate (TEOS)	$\text{Si}(\text{OC}_2\text{H}_5)_4$	98%	Sigma-Aldrich
Anhydrous sodium aluminate	$\text{NaAlO}_2$	41.383% $\text{Na}_2\text{O}$ , 58.604% $\text{Al}_2\text{O}_3$	Riedel-de Haën®
Hydrochloric acid	$\text{HCl}$	37%	Merck
Sodium hydroxide	$\text{NaOH}$	97% (pellets)	Carlo Erba
Cerium nitrate	$\text{Ce}(\text{NO}_3)_3 \cdot 6\text{H}_2\text{O}$	99.5%	Acros Organics
Commercial NaY	$\text{SiO}_2:\text{Al}_2\text{O}_3$	5.1:1	Alfa Aesar
Ammonium nitrate	$\text{NH}_4\text{NO}_3$	99% (AR grade)	QRëC™
2-Methylbut-3-yn-2-ol (MBOH)	$\text{C}_5\text{H}_8\text{O}$	99%	Fluka
Toluene	$\text{C}_7\text{H}_8$	99%	Fluka

### 3.2 Preparation of ion exchange (Ce-NaY-IE) and impregnation (Ce-NaY-IMP) samples

Cerium ions was introduced into zeolite Y by ion exchange and impregnation methods using a commercial NaY as parent NaY. The NaY first was dried at 110°C overnight before used. In the case of ion exchange, the sample was prepared according to Sahu et al. (2018). Parent NaY (1.03 g) was exchanged with  $\text{Ce}(\text{NO}_3)_3 \cdot 6\text{H}_2\text{O}$  solution (0.52 g dissolved in DI water 10.0 mL) by continuous stirring at 100°C for 1 h under reflux setup. The resultant sample was separated by centrifugation, washed with DI water and dried at 110°C overnight. The procedure was repeated three times and finally calcined at 550°C for 2 hours. The obtained solid was called “Ce-NaY-IE” where Ce, NaY and IE represent cerium, zeolite Y and ion exchange.

In the case of impregnation, the sample was prepared by the incipient wetness method, modified from Fillipe et al. (2011) and Kosri et al. (2017).  $\text{Ce}(\text{NO}_3)_3 \cdot 6\text{H}_2\text{O}$  (0.28 g) was dissolved in 1.2 mL of DI water and dropped slowly to 0.8 g of the dried NaY. The mixture was stirred for 10 minutes and sonicated in ultrasonic bath for further 10 minutes. The mixture was incubated at room temperature for 24 hours, dried at 110°C for 6 hours and calcined at 550°C for 2 hours. The obtained solid was denoted as “Ce-NaY-IMP” where Ce, NaY and IE represent cerium, zeolite Y and impregnation.

### 3.3 Synthesis of cerium-incorporated sample (Ce-NaY-INC)

The synthesis of cerium-incorporated zeolite Y was performed by a one pot synthesis with acidic co-hydrolysis followed by conventional basic media. The procedure was modified from Wu et al. (2010) and Gu et al. (2013). The gel composition of zeolite Y with the mole ratio of  $4.62\text{Na}_2\text{O} : \text{Al}_2\text{O}_3 : 10\text{SiO}_2 : 180\text{H}_2\text{O}$  was prepared according to (Mintova et al., 2016). The detail of one pot synthesis of zeolite Y is described in the Appendix. TEOS as Si source (6.25 g) and solution of  $\text{Ce}^{3+}$  prepared by dissolving  $\text{Ce}(\text{NO}_3)_3 \cdot 6\text{H}_2\text{O}$  (0.73 g) in DI water (3.05 g) are mixed and stirred vigorously. A solution of 0.24 M HCl was added dropwise under stirring to adjust the pH to 1. The stirring was continued for 2 hours. This solution is named solution A. Solution B was prepared from a mixture of anhydrous NaAlO<sub>2</sub> as Si source (0.55 g) and NaOH solution from sodium hydroxide pellet (1.37 g) dissolved in DI water (6.42 g). The mixture was stirred until clear before used. Afterward, solution B was slowly dropped into solution A under vigorous stirring. The combination was stirred further for 30 minutes and transferred into a Teflon-lined autoclave of 100 mL in volume. Then, it was aged at room temperature for 24 hours and finally crystallized at 90°C for 24 hours under a static condition. Then, the product was separated by centrifugation and washed with DI water several times until the pH of the supernatant was around 7. After that, the sample was dried at 110°C overnight. The obtained solid was designated as “Ce-NaY-INC” where Ce, NaY and INC stand for cerium, zeolite Y and incorporation.

## 3.4 Characterization

### 3.4.1 X-ray diffraction (XRD)

Phases of samples were investigated by X-ray diffraction (XRD, Bruker D8 ADVANCE) with a monochromatic light source Cu K $\alpha$  radiation ( $\lambda = 1.5418 \text{ \AA}$ ) operated at voltage and current of 40 kV and 40 mA, respectively. Before the measurement, each sample powder was spread evenly in the sample holder and pressed by glass to produce a smooth surface. The XRD patterns were collected with an increment of  $0.02^\circ$  at a scan rate of 0.2 s/step.

### 3.4.2 Fourier transform infrared spectroscopy (FTIR)

Functional groups and vibration bands of Ce-containing zeolites were analyzed by Fourier-transform infrared spectroscopy (FT-IR) on a Bruker Tensor 27 using attenuated total reflectance (ATR) mode. The sample powders were placed on the ATR crystal and firmly pressed by a pressure tower. The spectra were recorded in the  $1200 - 400 \text{ cm}^{-1}$  region at a resolution of  $4 \text{ cm}^{-1}$  for 64 scans.

### 3.4.3 Raman spectroscopy

Vibration states of the samples surface species were studied by Raman spectra. The operation was provided by FT-Raman spectrophotometer on Bruker VERTEX 70 with RAM II module. The wavelength and laser Hg-arc source power were 1064 nm and 150 mW, respectively. A liquid N<sub>2</sub> cooled photo diode type detector collected the Raman signal. The spectra were recorded in the  $800 - 200 \text{ cm}^{-1}$  region at a resolution of  $4 \text{ cm}^{-1}$  for 100 scans.

### 3.4.4 UV-Vis diffuse reflectance spectroscopy

Diffuse reflectance UV-Vis spectra (UV-DR) were measured with the Agilent Technologies UV-visible spectrophotometer modeled Cary 300. With double

beam mode, the diffuse reflectance (%R) spectra were recorded in the wavelength range of 200 - 800 nm. Before the measurement, each sample powder was filled in black sample holder and pressed by glass to produce a smooth surface. Then, a piece of cover glass was attached for holding the packed sample. PTFE (polytetrafluoroethylene) was used as reflectance standard material. The operations were performed at room temperature with scan rate of 600 nm/min, data interval 1 nm/0.1 second.

#### **3.4.5 Scanning electron microscopy (SEM)**

Morphology, crystallinity and particle size of all samples were investigated by scanning electron microscopy, SEM (JEOL modeled JSM-6010LV). Before imaging, each sample powder was spread on a carbon tape and coated with gold by sputtering to make it electrically conductive.

### **3.5 Catalytic activity testing by transformation of MBOH**

The reaction was conducted in a fixed bed reactor controlled by an automated bench unit at Carl von Ossietzky Universität Oldenburg, Germany. Firstly, each sample was ground and sieved into 200 - 315  $\mu\text{m}$  size range. The 0.200 grams of sample was activated by heating to 350°C and kept at this temperature for 4 hours under  $\text{N}_2$  flow. Then the temperature was lowered to 150°C. A reactant or MBOH (95 vol%) was mixed with toluene (5 vol% as an internal standard) and cooled to 13°C. Afterward, the mixture was vaporized and flowed over the sample by  $\text{N}_2$  carrier gas. The temperature was maintained at 150°C for catalytic activity test. The gas products were analyzed on-line by a gas chromatograph (Hewlett Packard, HP 5890 Series II with FID detector type). The data analysis was obtained from a calculation of MBOH

conversion ( $X_{\text{MBOH}}$ ), yield ( $Y$ ) and selectivity ( $S$ ) of each product from the transformation of MBOH by Equations 1-3, respectively.

$$X_{\text{MBOH}}(\%) = \frac{n_{\text{MBOH, in}} - n_{\text{MBOH, out}}}{n_{\text{MBOH, in}}} \times 100 \quad (1)$$

$$Y_{\text{P}}(\%) = \frac{A_{\text{P}}R_{\text{P}}/M_{\text{P}}}{\sum_{\text{K}} A_{\text{K}}R_{\text{K}}/M_{\text{K}}} \times 100 \quad (2)$$

$$S_{\text{P}}(\%) = \frac{Y_{\text{P}}}{X_{\text{MBOH}}} \times 100 \quad (3)$$

where  $A_{\text{P}}$ ,  $R_{\text{P}}$ ,  $M_{\text{P}}$ ,  $S_{\text{p}}$  and  $Y_{\text{P}}$  represent the area, response factor, mass, selectivity and yield of product P, respectively. While  $A_{\text{K}}$ ,  $R_{\text{K}}$  and  $M_{\text{K}}$  represent the area, response factor and mass of all components.

The MBOH reaction test apparatus used is set-up by a research group of Professor Frank Rößner. It consists of various parts as presented in Figure 3.1.

- A capillary with a length about 25 cm and diameter 0.3 cm for filling the mixture of MBOH and toluene (internal standard)
- A mass flow controller (MFC) for controlling the gas flow
- A pressure indicator (PI) for measuring pressure inside the system.
- An evaporator for feeding liquid MBOH to be vaporized.
- A reactor with tubular quartz tube for containing the solid catalyst
- A four-way valve for switching stream of the mixture from a bypass to the reactor path when a constant stream is established
- A gas chromatograph (GC) for gas analysis of the remained reactant and produced products
- A computer (PC) for setting up the condition and recording the data

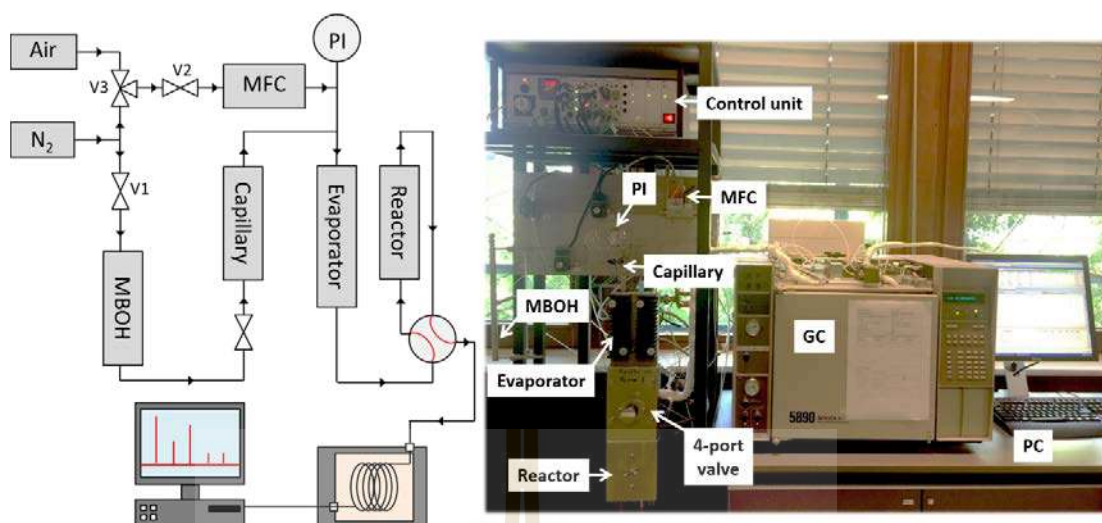


**Figure 3.1** Operation apparatus (the left scheme drawn by Sosa, N.).

### 3.6 References

- Fillipe A. C. G., Araújo, D. R., Silva, J. C. M., Macedo, J. L. d., Ghesti, G. F., Dias, S. C. L., Dias, A. J. and R. Filho, G. N. (2011). Effect of cerium loading on structure and morphology of modified Ce-USY zeolites. **Journal of the Brazilian Chemical Society**. 22: 1894-1902.
- Kosri, C., Deekamwong, K., Sophiphun, O., Osakoo, N., Chanlek, N., Föttinger, K. and Wittayakun, J. (2017). Comparison of Fe/HBEA catalysts from incipient wetness impregnation with various loading on phenol hydroxylation. **Reaction Kinetics, Mechanisms and Catalysis**. 121(2): 751-761.
- Mintova, S. and Barrier, N. (2016). Verified syntheses of zeolitic materials. **Commission of the International Zeolite Association**.
- Sahu, P., Eniyarppu, S., Ahmed, M., Sharma, D., and Sakthivel, A. (2018). Cerium ion-exchanged layered MCM-22: preparation, characterization and its application for esterification of fatty acids. **Journal of Porous Materials**. 25(4): 999-1005.

Wu, Y., Wang, J., Liu, P., Zhang, W., Gu, J. and Wang, X. (2010). Framework-substituted lanthanide MCM-22 zeolite: synthesis and characterization. **Journal of the American Chemical Society**. 132: 17989-17991.



## CHAPTER IV

### RESULTS AND DISCUSSION

#### 4.1 Phase analysis by X-ray diffraction

Figure 4.1 exhibits XRD patterns of the commercial zeolite NaY (NaY) and Ce-containing samples from different preparation methods including ion exchange (Ce-NaY-IE), impregnation (Ce-NaY-IMP) and incorporation (Ce-NaY-INC). The characteristic peaks at  $2\theta$  around 6.19, 10.11 and 11.86 degree (or reflections at 14.28, 8.75 and 7.46 Å) of faujasite framework (Treacy and Higgins, 2001; Mintova and Barrier 2016) are observed from all samples. The relative zeolite peaks intensities of Ce-NaY-IE and Ce-NaY-IMP samples are lower than that the parent NaY. The decrease intensities indicating the loss of crystallinity after calcination. Moreover, the decrease could be from X-ray absorption of Ce species (Fillipe et al., 2011). In addition, Lee et al. (2019) reported that the introduction of metal ions into zeolite Y, especially the Ce cations, further decreased the intensity of the peaks due to high ion-exchange selectivity. Nonetheless, the reduction in characteristic peaks of parent Y and modified Y zeolites are comparable to each other indicating that the original Y zeolite structure is retained.

In case of Ce-NaY-INC, the zeolite-peak intensities are the lowest. This could attribute from small crystal size and/or low crystallinity (Bunmai et al., 2018). Since, the addition in the Ce-NaY-INC was done through the acidic co-hydrolysis route, TEOS slowly hydrolyzed and polymerized in the presence of  $Ce^{3+}$  under acidic

condition. Such procedure could create the Si-O-Ce-O-Si (Wu et al., 2010). However, the incorporation of metal ions into the zeolite framework or isomorphous substitution is restricted due to solubility and specific chemical behavior of the tetrahedral (T) ionic radii precursors in the synthesis mixture (Mizuno, 2009). This Ce insertion might cause changes in zeolite crystallization and finally distribution of amorphous composition.

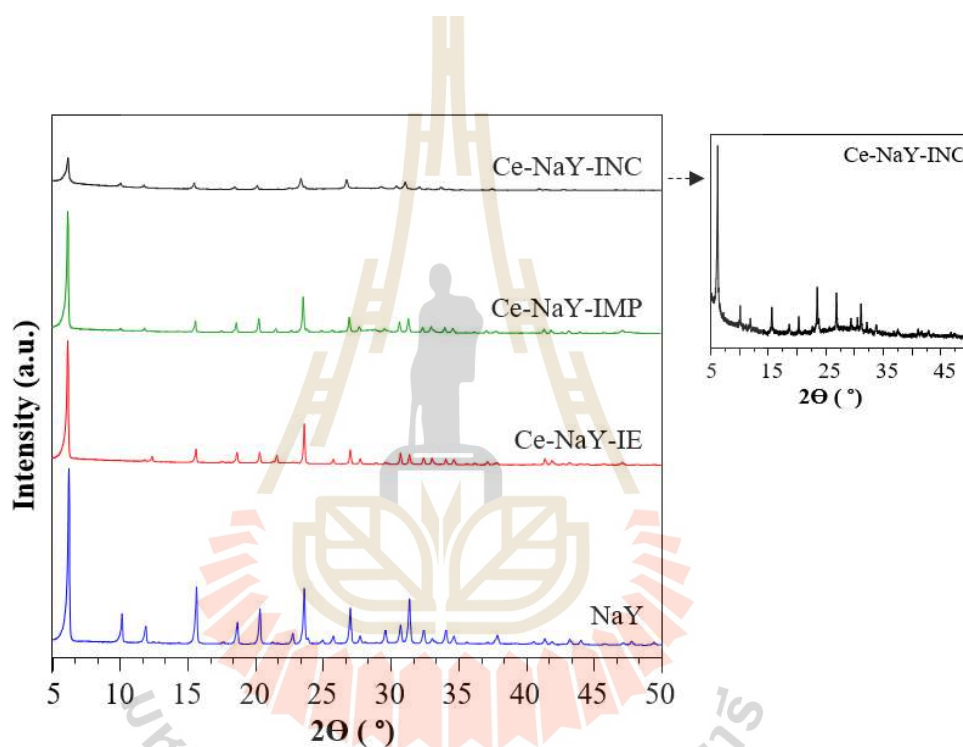


**Figure 4.1** XRD patterns of NaY, Ce-NaY-IE, Ce-NaY-IMP and Ce-NaY-INC.

Apart from that, peaks corresponding to cerium oxide or other Ce-based phases are not observed in all patterns. In Ce-NaY-IE case, Ce in the form of ions ( $\text{Ce}^{3+}$ ) could present in the exchangeable sites with uniform distribution. This hypothesis is supported by Sahu et al. (2018) owing to the absence of peak corresponding to  $\text{CeO}_2$ , even though they conducted cerium exchange four times on MCM-22.

From Ce-NaY-IMP, Ce is loaded by incipient wetness impregnation. The calcination at 550°C is enough to transform Ce species to oxides (Borges et al., 2013). However, characteristic peaks corresponding to CeO<sub>2</sub> structure ( $2\theta = 28^\circ, 33^\circ$  and  $48^\circ$ ) are not observed, implying a good dispersion. The same results were obtained in Saceda et al. (2012) work, they suggested that the peaks CeO<sub>2</sub> could overlap with the peaks at similar position from the zeolites. Moreira et al. (2007) prepared Ce on Ultra Stable zeolite Y with proton form (HUSY) by incipient wetness impregnation and obtained ambiguous results similar to this work. From Rietveld Refinements (by means of the FULLPROF software), they explained that Ce existed in both separate CeO<sub>2</sub> phase and exchanged ions.

In the case of Ce-NaY-INC, XRD pattern cannot provide the formation of Ce in this work. In the past, Mohammad et al. (2005) noticed cerium silicate [Ce<sub>2</sub>(Si<sub>2</sub>O<sub>7</sub>)] phase from small diffraction peaks at d values of 3.169, 3.122, 2.954 and 1.956 Å as cerium incorporated species in mordenite zeolite.

From the diffractograms, it can be concluded that all introducing methods of Ce into zeolite Y affect framework crystallinity in different ways. In addition, it can be roughly explained the location of Ce.

## 4.2 Functional groups and forms of Ce species by spectroscopy

### 4.2.1 Fourier-transform infrared spectroscopy

Figure 4.2 illustrates FTIR spectra in the range of 1200 to 400 cm<sup>-1</sup> which is the range of the zeolite vibrations. All spectra are similar in shape but different in frequency and intensity. Comparing with the dash lines position of NaY, the spectra of all Ce-containing zeolite materials show the vibrational bands around 453, 712 and

992  $\text{cm}^{-1}$  corresponding to  $\text{TO}_4$  ( $T = \text{Si}, \text{Al}$ ) bending, symmetrical and asymmetrical stretching of internal tetrahedron linkages (Flanigen, 1976). These vibrations are observed for all aluminosilicates including amorphous precursors and the primary units of zeolite. While the peaks (dash lines with arrow) around 578, 789 and the shoulder at 1145  $\text{cm}^{-1}$  are attributed to the double 6-membered ring (D6R), symmetrical and asymmetrical stretching of external linkages between  $\text{TO}_4$  tetrahedra of faujasite framework, respectively (Flanigen, 1976). However, differences among Ce-NaY-IE and Ce-NaY-IMP with parent NaY are clearly seen at the band and shoulder in the region of 900-1200  $\text{cm}^{-1}$ . The frequencies shifts are sensitive from framework Si/Al ratio (Miecznikowski and Hanuza, 1985). The shifts attributed from calcination and/or ion-exchange preparation steps that lead to structural collapse (Saceda et al., 2012) and the acidic impregnated solution of cerium nitrate hexahydrate step that lead to partial dealumination of parent zeolite (Beyer, 2002).

Kulprathipanja (2010) explained that the existence of Al in the framework certainly changes the T-O-T bond angles due to smaller size and different charge density of the Al atoms compared to Si. This results in a shift in frequency for T-O-T asymmetric, symmetric stretching modes as well as structural unit vibrations like D6R that exhibit a shift to higher frequencies as the Al content is decreased. In the case of Ce-NaY-INC, the shifts cannot be compared with Ce-NaY-IE and Ce-NaY-IMP spectra since this sample was not obtained from post-modified NaY. However, the spectrum of Ce-NaY-INC is mainly raised from amorphous phase as aforementioned in section 4.1.

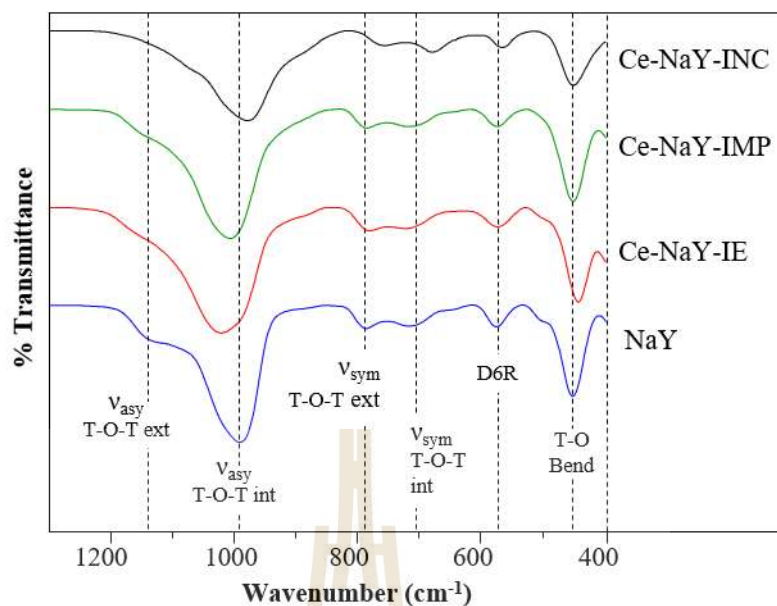


**Figure 4.2** FTIR spectra of NaY, Ce-NaY-IE, Ce-NaY-IMP and Ce-NaY-INC.

The discussion of characteristic vibrations and Si/Al shifts is the information of short-range in zeolite structure (Miecznikowski and Hanuza, 1985). Since, there are some differences among all spectra. That means modified materials show different situation of zeolite characters compatible with previous XRD analysis that reveals long-range of zeolite structure.

#### 4.2.2 Raman spectroscopy

Figure 4.3 presents Raman spectra in the range of 800 to 200  $\text{cm}^{-1}$ . All sample give different spectra. The band corresponding to Ce species is observed only from Ce-NaY-IMP at 464  $\text{cm}^{-1}$ . This peak is assigned to symmetric vibration mode of oxygen at neighboring positions of the  $\text{Ce}^{4+}$  ions (O – Ce – O) that is characteristic of  $F_{2g}$  vibration of  $\text{CeO}_2$  or ceria fluorite-type lattice (Schmitt et al., 2020). The band of ceria is not observed from Ce-NaY-IE. This result is similar to the work of Moreira et al. (2007) work. As mentioned in XRD analysis, they did not see the  $\text{CeO}_2$

characteristic band in Raman spectrum of Ce loaded on HUSY by ion exchange. This result might point to the absence of a separate phase of  $\text{CeO}_2$ .

In the case of Ce-NaY-INC, Ce species was not observed from the spectrum as well. Strunk et al. (2011) have remarked that the absence of the Raman signal cannot be ascribed to the insufficient amount of ceria since their sample contained  $\sim 10$  wt % ceria in mesoporous silica, giving further indication that the ceria in the sample is not crystalline. Note that the presence of Ce species of Ce-NaY-IE and Ce-NaY-INC is further studied by UV-Vis diffuse reflectance spectroscopy in the next section.

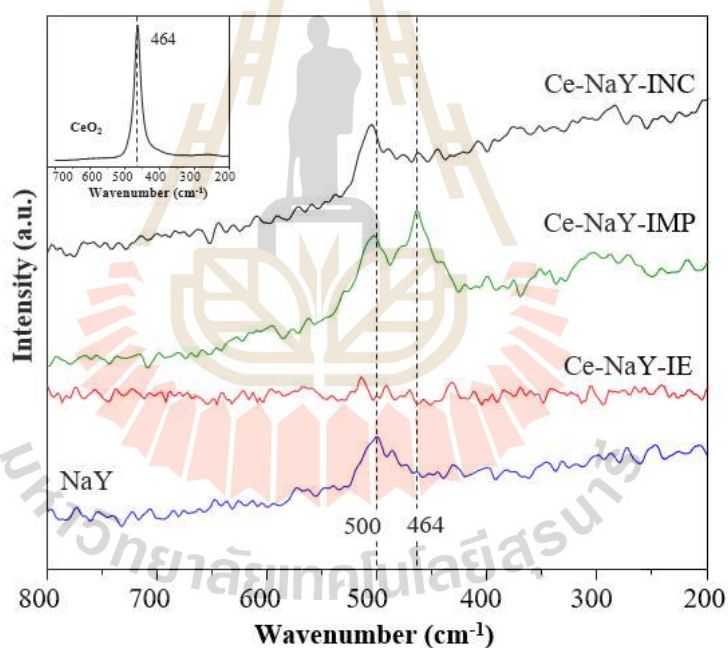


**Figure 4.3** Raman spectra of NaY, Ce-NaY-IE, Ce-NaY-IMP, Ce-NaY-INC and  $\text{CeO}_2$  (inset Figure).

Another Raman band at  $\sim 500$  cm<sup>-1</sup> in Ce-NaY-IMP and Ce-NaY-INC spectra is attributed to T-O-T bending of zeolite 4-membered rings. This band is correlated

to the ring size, average T–O–T angle and the Si/Al ratio in the crystalline framework (Wang et al., 2013).

#### 4.2.3 UV–Vis diffuse reflectance spectroscopy (UV-DR)

Figure 4.4 exhibits the UV-DR spectra of all samples together with the spectrum of CeO<sub>2</sub>. The bare ceria shows a large absorption band around 315 nm (dash line) originates from a charge transfer transition from O 2p to Ce 4f (Sahu et al., 2018). The modified samples, except Ce-NaY-IMP, display different in the wavelength of peak maximum compared to CeO<sub>2</sub>. While Ce-NaY-IMP reveals the similar peak shape to ceria, that attributed to CeO<sub>2</sub> phase containing as mentioned in Raman spectrum. However, this might be unusual. From earlier researches, the absorption results of porous-supported or material-contained CeO<sub>2</sub> of Bensalem et al. (1992); Laha et al. (2002); Krishna Reddy et al. (2009); Strunk et al. (2011); Mortola et al., (2011) provided the different in spectra comparing to pure CeO<sub>2</sub>. That probably caused by some interaction between the oxide species and materials.

Ce-NaY-IE exhibits a peak shift which ascribes the formation of small cerium oxide clusters, as cerium ions in exchangeable sited undergo calcination and dehydration process (Roth et al., 2016). In addition, Bensalem et al. (1992) who worked on varying CeO<sub>2</sub> amount supported on silica, have remarked that the shift towards shorter wavelengths (blue shift) could be explained by the predominance of Ce<sup>IV</sup>-oxygen charge transfers occurring on low coordination Ce<sup>IV</sup> ions.

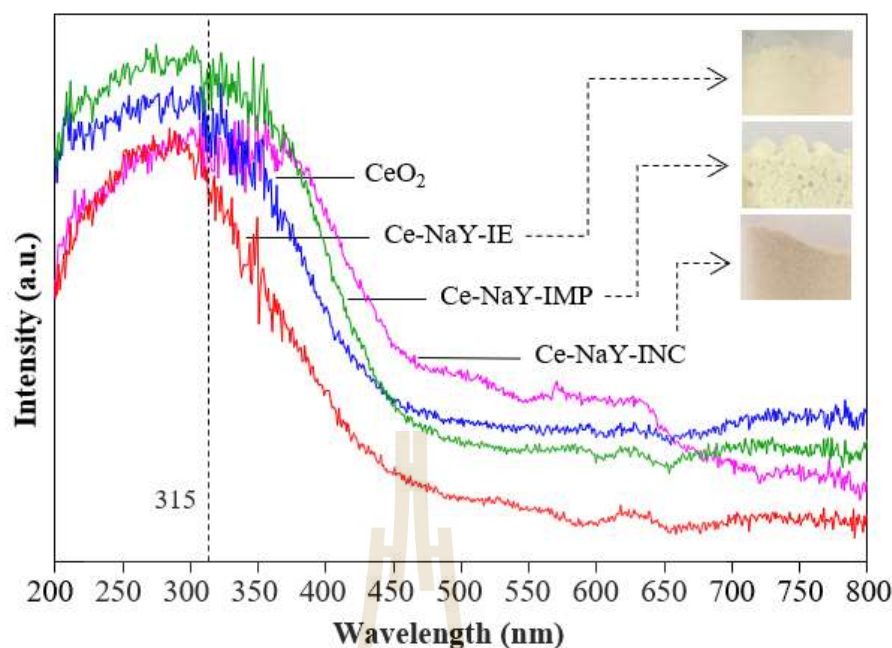


**Figure 4.4** UV-DR spectra of CeO<sub>2</sub>, Ce-NaY-IE, Ce-NaY-IMP and Ce-NaY-INC with the powder color of modified NaY samples (inset images).

A broader absorption, comparing to all samples, is observed in Ce-NaY-INC spectrum. Apart from the peak corresponding charge transfer transition, non-smooth baseline is observed. It might be caused by non-uniform color and sand-like texture of obtained Ce-NaY-INC sample (inset image). This result confirms the presence of amorphous aluminosilicate consistent with the XRD and FT-IR results.

From the Ce phase investigation by 2 above techniques, the Raman spectra distinguish the formation of CeO<sub>2</sub> only in Ce-NaY-IMP sample, Meanwhile, all UV-DR spectra present the Ce<sup>4+</sup> absorption transition. It can be concluded that all samples have cerium in CeO<sub>2</sub> form. This species might locate in various positions on zeolite Y attributed from different preparation strategies. However, the location of Ce species can be assumed from the literatures;

- **Ion exchange method** could provide CeO<sub>2</sub> inside supercage at exchangeable positions of zeolite through ion exchange followed by calcination processes as proposed by Li et al. (2015).
- **Incipient wetness impregnation method** could provide CeO<sub>2</sub> on the external surface of zeolite as Saceda et al. (2012) suggested. By N<sub>2</sub>-sorption, they found the decreasing of surface area after Ce adding. In addition, calcination step gives the driving force for Ce<sup>3+</sup> migration then form oxides in exchange positions (Moreira et al., 2007).
- **Incorporation method** could provide CeO<sub>2</sub>, but the location cannot be defined for now. On the other way, Ce might not incorporate in TO<sub>4</sub> unit position. That resulted from non-success zeolite synthesis as the expose of amorphous phase.

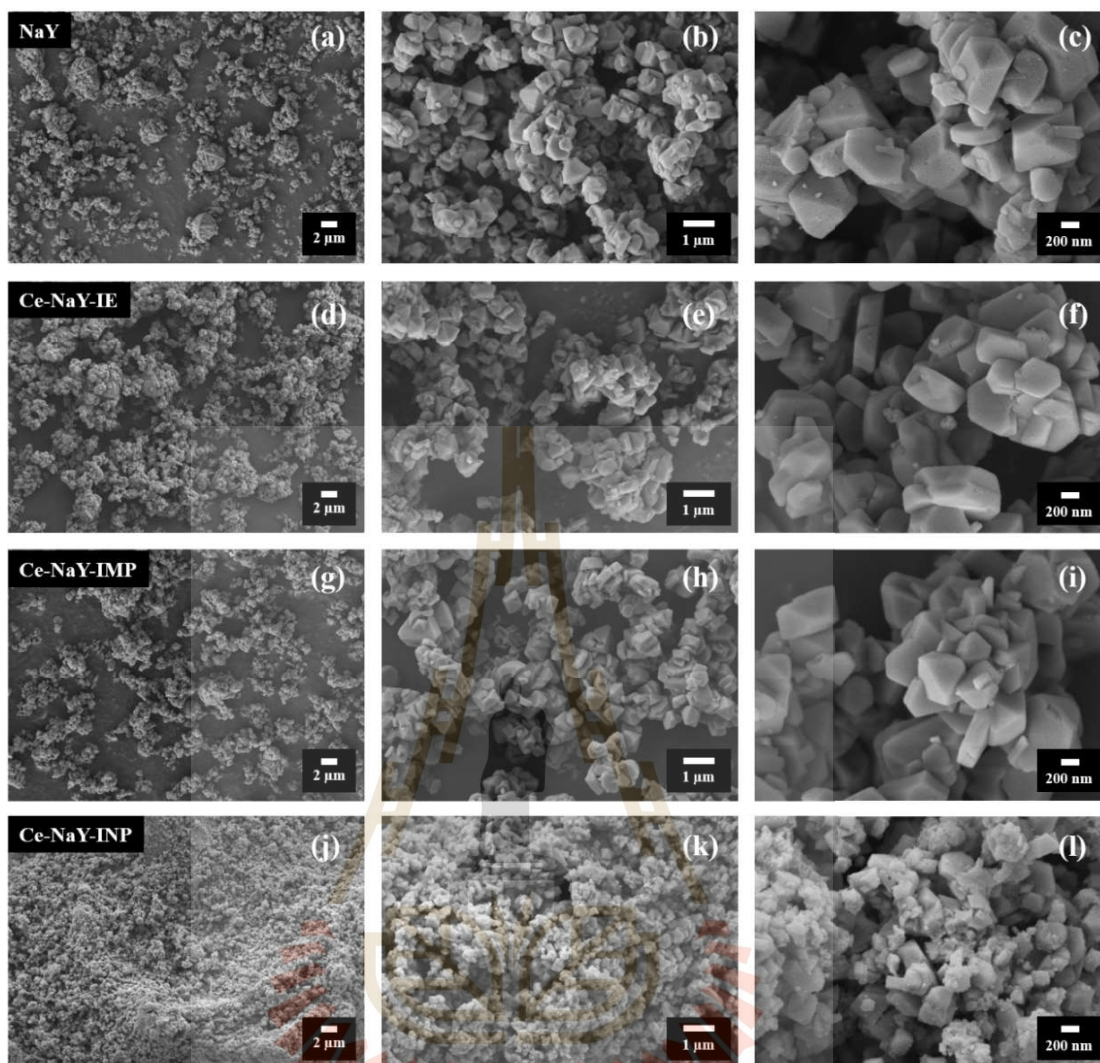
### 4.3 Morphology observation by Scanning Electron Microscopy

Figure 4.5 shows SEM images of all samples with different magnitudes. The parent NaY has various in shape and size of crystal (Figure 4.5(a) – (c)). Increasing of magnification, an agglomeration of polycrystalline is observed in Figure 4.5(b) followed by polygonal and plate-like morphology are monitored in Figure 4.5c. The crystal sizes of NaY are approximately range from 500 nm to 1 μm. In addition, the highest magnification from Figure 4.5(c) displays the characteristic porosity of zeolite.

For Ce-NaY-IE and Ce-NaY-IMP, the micrographs reveal similar appearance to NaY as presented in Figure 4.5(d) – (f) and 4.5(g) – (i), respectively. The crystallinity with clear faces and edges of zeolite are preserved after Ce introduction

by incipient wetness impregnation and ion exchange methods. Unfortunately, the  $\text{CeO}_2$  particles are not found in the images. However, it can be concluded that the morphology of parent NaY did not change after Ce loading via those post modifications.

In the case of Ce-NaY-INC, significant difference is appeared. With the lowest magnitude, Figure 4.5(j) displays the occurrence of sample powder. The morphology shape and size cannot be described clearly. Figure 4.5(k) shows very low crystallinity comparing to others. However, small particle of the zeolite crystal and amorphous are revealed in Figure 4.5(j) consistent with XRD that Ce-NaY-INC has mix phases. Some polygonal shape of zeolite ranges around 200 - 400 nm, implying the smallest particle size. In addition, porosity is also observed on the crystal surface. It can be concluded that Ce adding simultaneously with the zeolite synthesis provides both characteristic of zeolite and amorphous aluminosilicate.



**Figure 4.5** SEM micrographs of NaY (a) – (c), Ce-NaY-IE (d) – (f), Ce-NaY-IMP (g) – (i) and Ce-NaY-INP (j) – (l).

#### 4.4 Catalytic transformation of methylbutynol (MBOH)

The acid-base properties of all samples were characterized through the transformation of MBOH under reaction temperature of 150°C with catalyst amount of 0.200 g. The catalytic activity in term of conversion and selectivity versus time on stream are presented in Figure 4.6 and 4.7. In Figure 4.6, the MBOH conversions of NaY, Ce-NaY-IE, Ce-NaY-IMP and Ce-NaY-INC are 9, 13, 18 and 4%, respectively, in the first 25 min. After that, the catalysts exhibit different activity. The conversion of NaY swings, then, slightly decreases after 90 min until meet 4%. Comparing to the similar work of Supanathanon et al. (2012), they also obtained low conversion with a steady value around 4%. This difference is mainly resulted from the lower reaction temperature and less catalyst amount of their condition (120°C, 0.020 g).

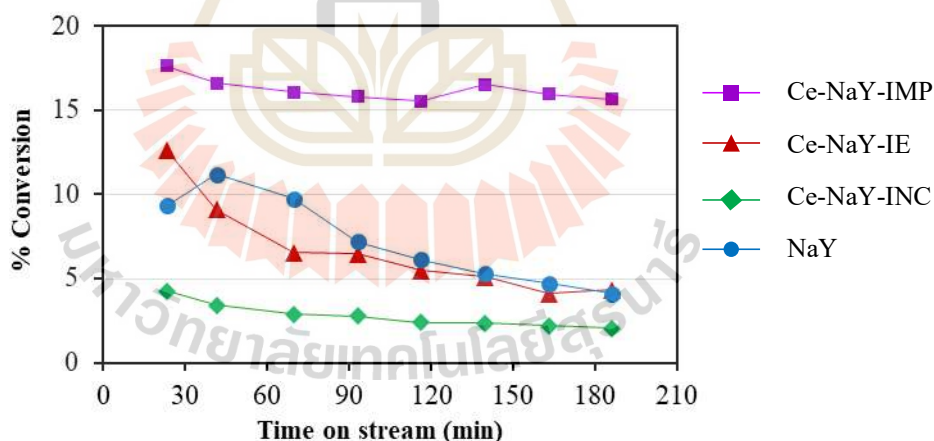


**Figure 4.6** MBOH conversion of NaY, Ce-NaY-IE, Ce-NaY-IMP and Ce-NaY-INC.

In case of Ce-containing catalysts, the conversion of Ce-NaY-IE continuously decreases with time on stream from 13 to 4%. Meanwhile, Ce-NaY-IMP shows highest conversion and steady numbers between 16 - 18%. For Ce-NaY-INC, the conversion slightly decreases and finally displays only 2%. It can be noticed that the

modification of zeolite Y with different introduced Ce methods changes the catalytic activity of the materials. Which are explained and discussed in more detail together with the results of products selectivity.

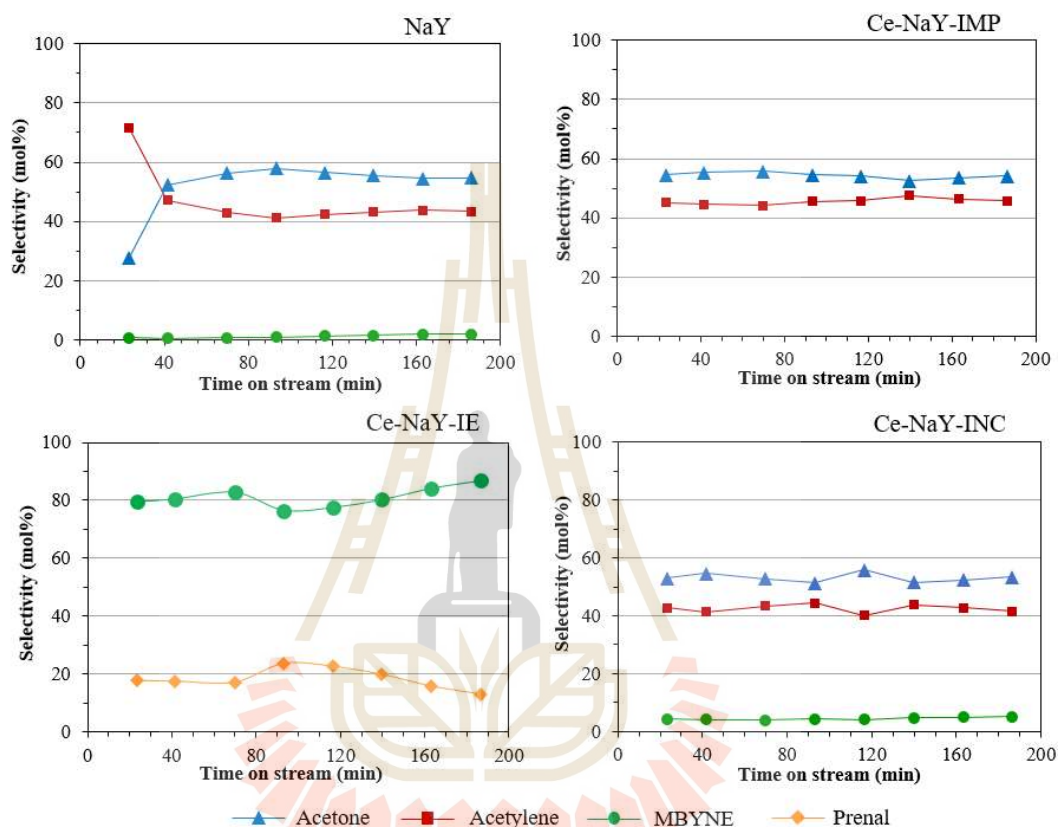


**Figure 4.7** Products selectivity from MBOH conversion of NaY, Ce-NaY-IE, Ce-NaY-IMP and Ce-NaY-INC samples.

Figure 4.7 presents the selectivity versus time on stream. The NaY and Ce-NaY-INC contains acetone and acetylene as major products with small amount of MBYNE. While the Ce-NaY-IE has MBYNE as main product and some amount of prenal. In the case of Ce-NaY-IMP, only acetone and acetylene are displayed. The products selectivity from MBOH decomposition depend on active sites within the catalyst; acetone and acetylene are generated by basic sites; on the other hand, acidic

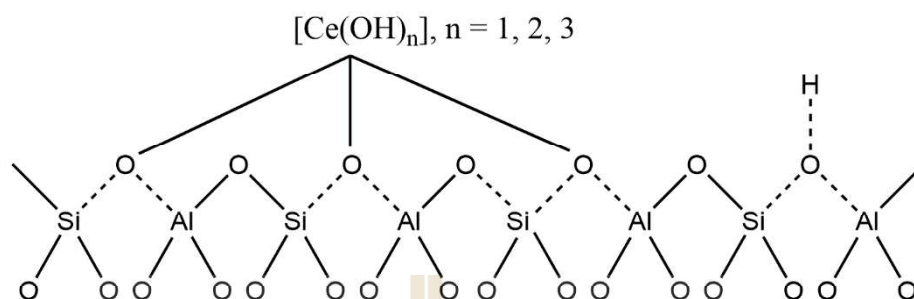
sites produce MBYNE and prenal; in addition, coordinative unsaturated sites turn MBOH into MIPK and HMB which the latest do not take place in this work.

So, the surface of the NaY zeolite contains predominantly basic sites and a very small number of acidic sites. The basic reactivity of zeolites is contributed from intrinsic oxygen atoms in the framework, defined as Lewis basic sites that form acid-base pairs with the charge compensating cations (Barthomeuf, 1996). These results are similar to Supanathanon et al. (2012). However, the MBYNE selectivity of their report was almost 20%, significantly higher than that of this work. It might be due to different in Si/Al ratios and amount of silanol group which provide Lewis acid-base pairs and Brønsted acid, respectively (Huang and Kaliaguine, 1993). Apart from that, the selectivity distribution of NaY catalyst in this work reveals the molar ratio between acetone and acetylene higher than the theoretical. In fact, the value is equal to 1.00 owing to they generated from the cleavage of MBOH molecules. Nonetheless, the value can be less than 1.00 because of aldol condensation of acetone producing products which adsorbed strongly on the surface (Aramendía et al., 1999). The conversed results still could not be explained.

For Ce-NaY-IE, MBYNE is detected as superior product and inferior of prenal which means the reaction happened through acid-catalyzed pathway. According Falabella et al. (2013), Ce-introduced by ion exchange could produce dissociative H<sup>+</sup> via dehydration among hydrothermal treatment of hydrated cerium ions as depicted in equation.



That further attributes the formation of Bronsted acid sites through bridged hydroxyls as show below (Du et al., 2013).



In addition, these acidic sites could catalyze polymerization of MBOH, or secondary reactions lead to coke deposit on the surface of catalyst (Kulawong et al., 2015). That caused decrease in MBOH conversion of Ce-NaY-IE over time (Figure 4.6). The coke formation of Ce-NaY-IE is presented in Figure 4.8 which significant serious among other Ce-containing catalyst. In other word, the ion exchange method of Ce into zeolite Y does not provide the improvement of catalytic activity in term of MBOH conversion. However, the process turns parent NaY which is preferred-basic into acid property of Ce-NaY-IE.

Besides, Ce-introduced NaY by impregnation, Ce-NaY-IMP, provided the higher MBOH conversion than that of NaY and more steady activity. In addition, Ce-NaY-IMP produce acetone and acetylene, thus, it contains basic-catalyzed property. The conversion improvement is attributed from an enhancement of Lewis basic sites resulted from oxygen vacancies of  $\text{CeO}_2$  phase (Chen et al., 2017) containing in Ce-NaY-IMP sample. The catalytic activity of ceria supports the existence of  $\text{Ce}^{4+}$  species with above Raman and UV-DR spectra results. Nevertheless, the selectivity of acid-catalyzed products like parent NaY are not observed. This result indicates that impregnation with cerium suppressed the acidic sites of NaY. As Supanathanon et al.,

(2012) reported the absence of acidic products from the potassium-impregnated on zeolite Y.

For Ce-NaY-INC, the catalyst with lowest MBOH conversion, carries products of acetone and acetylene with small amount of MBYNE. So, the sample has basic sites as major activity and acidic sites as minor. From previous characterizations including XRD pattern, Raman together with UV-DR spectra of Ce-NaY-INC, they disclose the mix phases of FAU zeolite, amorphous aluminosilicate and CeO<sub>2</sub> in the sample. However, the origination of activity cannot be clearly defined at this time. Since the conversion of Ce-NaY-INC is less than 5%, the error could be existed from the limitation of operation system (AlSawalha and Rößner, 2008). That means the reaction test of MBOH transformation cannot distinguish the surface reactivity of Ce-NaY-INC. Thus, it can be assumed that the adding of Ce into zeolite by incorporation synthesis exhibits non-active catalyst in this case.

Ce-containing zeolite from different introduced method significantly affected the location and species of cerium. Consequently, lead to the differences of catalytic activity by MBOH transformation reaction testing in term of conversion tendency and/or product selectivity.

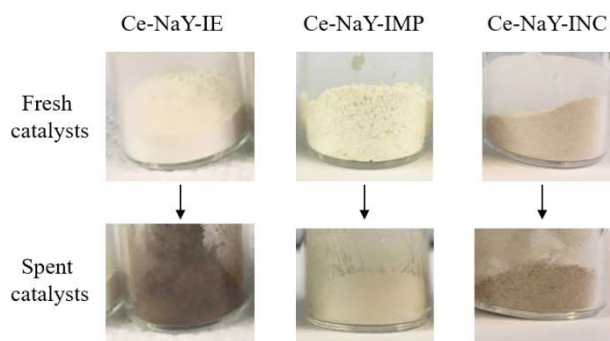


**Figure 4.8** The color of catalyst powder before and after reaction testing.

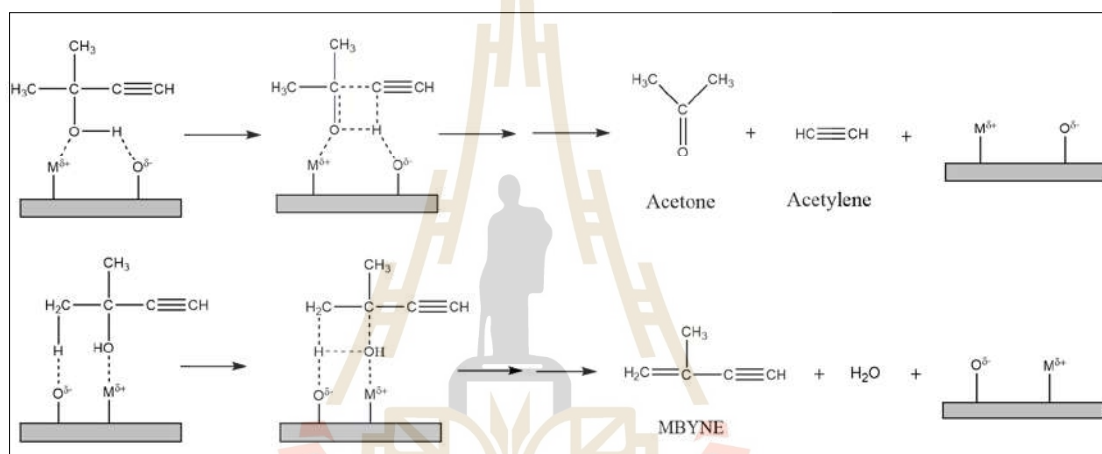


**Figure 4.9** Mechanism schemes of Lewis acid-base pair catalyze the decomposition of MBOH.

Herein, Figure 4.9 illustrates the mechanism schemes of acetone, acetylene and MBYNE formation through different acidic and basic pathways purposed by Huang and Kaliaguine (1993). After MBOH adsorption on surface of catalyst, both Lewis acid-base pairs take part in mechanisms. The phenomena between 2 reactions are mainly caused by the different acid and base strength. In case of the strong basic site, it can abstract a hydrogen atom of MBOH. Then cleavage reaction takes place and finally resulting the formation of acetone and acetylene. On the other hand of the strong Lewis acidity, one hydrogen atom of  $\text{CH}_3$  could be directly captured by the OH

group from MBOH itself, which is activated by the Lewis acid site or charge compensating cation of zeolite catalyst. After that, the dehydration of MBOH is happened results in the formation of MBYNE.

Another mechanism of MBYNE production is revealed in Figure 4.10 which purposed by AlSawalha and Rößner (2008). It carried out through the silanol group on catalyst surface. The authors explained that the acidic hydrogen on the surface is attacked by the alcoholic oxygen of MBOH form a transition state. Then water molecule is eliminated, and the acid site is restored. In addition, the Bronsted acid sites from bridged hydroxyl groups are also active for the formation of MBYNE.

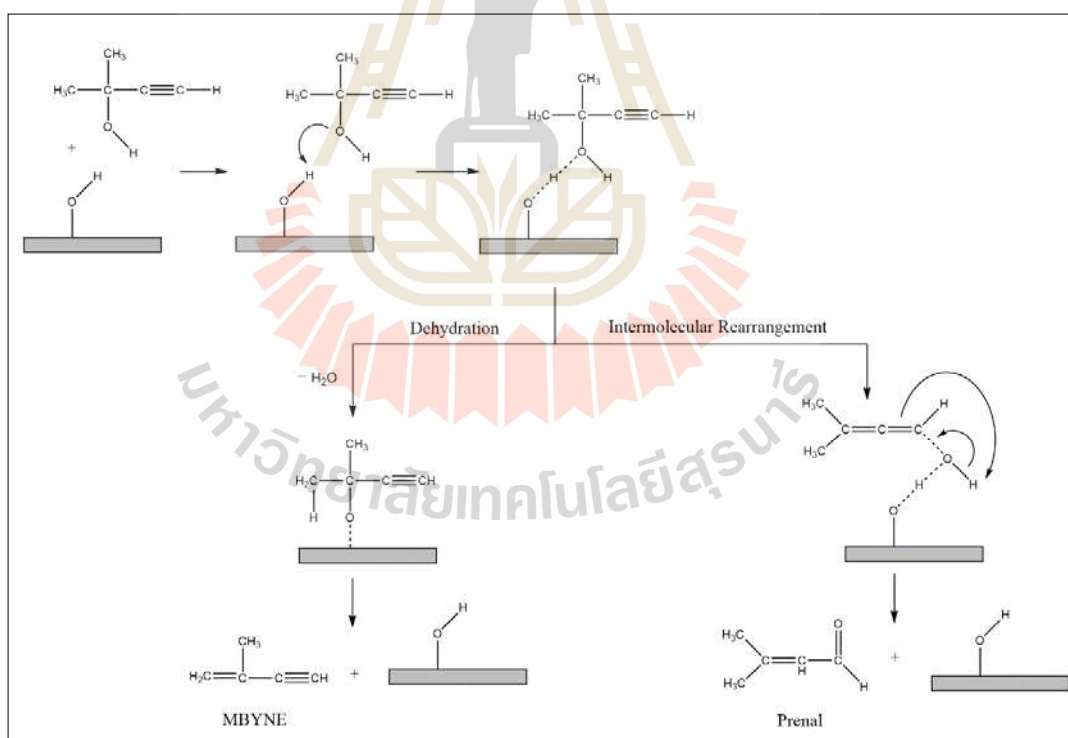


**Figure 4.10** Mechanism schemes of an acidic hydrogen on catalyst surface catalyze the decomposition of MBOH.

## 4.5 References

- AlSawalha, M. and Rößner, F. (2008). Characterization of surface properties of silica alumina by catalytic conversion of methylbutynol. **Сорбционные и хроматографические процессы**. 8(2): 192-201.
- Aramendía, M. A., Boráu, V., García, I. M., Jiménez, C., Marinas, A., Marinas, J. M., Porras, A. and Urbano, F. J. (1999). Comparison of different organic test reactions over acid–base catalysts. **Applied Catalysis A: General**. 184(1): 115-125.
- Barthomeuf, D. (1996). Basic Zeolites: Characterization and Uses in Adsorption and Catalysis. **Catalysis Reviews**. 38(4): 521-612.
- Belaabed, R., Elknidri, H., Elkhalfaouy, R., Addaou, A., Laajab, A. and Lahsini, A. (2017). Zeolite Y synthesis without organic template: The effect of synthesis parameters. **Journal of Materials and Environmental Science**. 8: 3550-3555.
- Bensalem, A., Muller, J. C. and Bozon-Verduraz, F. (1992). Faraday communications. From bulk CeO<sub>2</sub> to supported cerium–oxygen clusters: a diffuse reflectance approach. **Journal of the Chemical Society, Faraday Transactions**. 88(1): 153-154.
- Beyer, H. K. (2002). Dealumination Techniques for Zeolites. In Post-Synthesis Modification I: 203-255. **Springer Berlin Heidelberg, Heidelberg**.
- Borges, L. D., Moura, N. N., Costa, A. A., Braga, P. R. S., Dias, J. A., Dias, S. C. L., de Macedo, J. L. and Ghesti, G. F. (2013). Investigation of biodiesel production by HUSY and Ce/HUSY zeolites: Influence of structural and acidity parameters. **Applied Catalysis A: General**. 450: 114-119.

- Bunmai, K., Osakoo, N., Deekamwong, K., Rongchapo, W., Keawkumay, C., Chanlek, N., Prayoonpokarach, S. and Wittayakun, J. (2018). Extraction of silica from cogon grass and utilization for synthesis of zeolite NaY by conventional and microwave-assisted hydrothermal methods. **Journal of the Taiwan Institute of Chemical Engineers**. 83: 152-158.
- Chen, W., Ran, R., Weng, D., Wu, X., Zhong, J. and Han, S. (2017). Influence of morphology on basicity of CeO<sub>2</sub> and its use in 2-chloroethyl ethyl sulfide degradation. **Journal of Rare Earths**. 35(10): 970-976.
- Du, X., Gao, X., Zhang, H., Li, X. and Liu, P. (2013). Effect of cation location on the hydrothermal stability of rare earth-exchanged Y zeolites. **Catalysis Communications**. 35: 17-22.
- Fillipe A. C. G., Araújo, D. R., Silva, J. C. M., Macedo, J. L. d., Ghesti, G. F., Dias, S. C. L., Dias, A. J. and R. Filho, G. N. (2011). Effect of cerium loading on structure and morphology of modified Ce-USY zeolites. **Journal of the Brazilian Chemical Society**. 22: 1894-1902.
- Flanigen, E. M. (1976) Structural analysis by infrared spectroscopy. **ACS Monograph**. 171: 80-117.
- Huang, M. and Kaliaguine, S. (1993). Reactions of methylbutynol on alkali-exchanged zeolites. A Lewis acid-base selectivity study. **Catalysis Letters**. 18(4): 373-389.
- Krishna, K., Bueno-López, A., Makkee, M. and Moulijn, J. A. (2007). Potential rare earth modified CeO<sub>2</sub> catalysts for soot oxidation: I. Characterisation and catalytic activity with O<sub>2</sub>. **Applied Catalysis B: Environmental**. 75(3): 189-200.

- Krishna Reddy, J., Suresh, G., Hymavathi, C. H., Durga Kumari, V. and Subrahmanyam, M. (2009). Ce (III) species supported zeolites as novel photocatalysts for hydrogen production from water. **Catalysis Today**. 141(1): 89-93.
- Kulprathipanja, S. (2010). Zeolite in industrial separation and catalysis. **Wiley-VCH Verlag GmbH & Co. KGaA., Weinheim.**
- Kulawong, S., Prayoonpokarach, S., Roessner, F. and Wittayakun, J. (2015). Acidity of Modified Mordenites Synthesized from Rice Husk Silica and Catalytic Transformation of Methylbutynol. **Química Nova**. 38: 191-195.
- Laha, S. C., Mukherjee, P., Sainkar, S. R. and Kumar, R. (2002). Cerium containing MCM-41-type mesoporous materials and their acidic and redox catalytic properties. **Journal of Catalysis**. 207: 213-223.
- Lee, K., Wang, H., Karakalos, S., Tsilomelekis, G. and Valla, J. (2019). Adsorptive Desulfurization of 4,6-Dimethyldibenzothiophene on Bimetallic Mesoporous Y Zeolites: Effects of Cu and Ce Composition and Configuration. **Industrial & Engineering Chemistry Research**. 58: 18301–18312.
- Li, J., Zeng, P., Zhao, L., Ren, S., Guo, Q., Zhao, H., Wang, B., Liu, H., Pang, X., Gao, X. and Shen, B. (2015). Tuning of acidity in CeY catalytic cracking catalysts by controlling the migration of Ce in the ion exchange step through valence changes. **Journal of Catalysis**. 329: 441-448.
- Miecznikowski, A. and Hanuza, J. (1985) Application of the long chain approach to the structure and vibrational spectra of X and Y zeolites. **Zeolites**. 5: 188-193.
- Mintova, S. and Barrier, N. (Editor) (2016). Verified syntheses of zeolitic materials (2<sup>nd</sup> edition). **Commission of the International Zeolite Association.**

- Mizuno, N. (Editor) (2009) *Modern Heterogeneous Oxidation Catalysis: Design, Reactions and Characterization*. **WILEY-VCH Verlag GmbH & Co. KGaA., Weinheim.**
- Mohamed, M. M., Salama, T. M., Othman, A. I. and El-Shobaky, G. A. (2005). Low temperature water-gas shift reaction on cerium containing mordenites prepared by different methods. **Applied Catalysis A: General**. 279(1): 23-33.
- Moreira, C. R., Pereira, M. M., Alcobé, X., Homs, N., Llorca, J., Fierro, J. L. G. and Ramírez de la Piscina, P. (2007). Nature and location of cerium in Ce-loaded Y zeolites as revealed by HRTEM and spectroscopic techniques. **Microporous and Mesoporous Materials**. 100(1): 276-286.
- Mortola, V. B., Damyanova, S., Zanchet, D. and Bueno, J. M. C. (2011). Surface and structural features of Pt/CeO<sub>2</sub>-La<sub>2</sub>O<sub>3</sub>-Al<sub>2</sub>O<sub>3</sub> catalysts for partial oxidation and steam reforming of methane. **Applied Catalysis B: Environmental**. 107(3): 221-236.
- Novikova, L., Roessner, F., Belchinskaya, L., AlSawalha, M. and Krupskaya, V. (2014). Study of surface acid–base properties of natural clays and zeolites by the conversion of 2-methylbut-3-yn-2-ol. **Applied Clay Science**. 101: 229-236.
- Roth, W. J., Gil, B., Makowski, W., Sławek, A., Korzeniowska, A., Grzybek, J., Siwek, M. and Michorczyk, P. (2016). Framework-substituted cerium MCM-22 zeolite and its interlayer expanded derivative MWW-IEZ. **Catalysis Science & Technology**. 6(8): 2742-2753.
- Saceda, J.-J. F., Rintramee, K., Khabuanchalad, S., Prayoonpokarach, S., de Leon, R. L. and Wittayakun, J. (2012). Properties of zeolite Y in various forms and

utilization as catalysts or supports for cerium oxide in ethanol oxidation.

**Journal of Industrial and Engineering Chemistry.** 18(1): 420-424.

Sahu, P., Eniyarppu, S., Ahmed, M., Sharma, D. and Sakthivel, A. (2018). Cerium ion-exchanged layered MCM-22: preparation, characterization and its application for esterification of fatty acids. **Journal of Porous Materials.** 25(4): 999-1005.

Schmitt, R., Nanning, A., Kraynis, O., Korobko, R., Frenkel, A. I., Lubomirsky, I., Haile, S. M. and Rupp, J. L. M. (2020). A review of defect structure and chemistry in ceria and its solid solutions. **Chemical Society Reviews.** 49(2): 554-592.

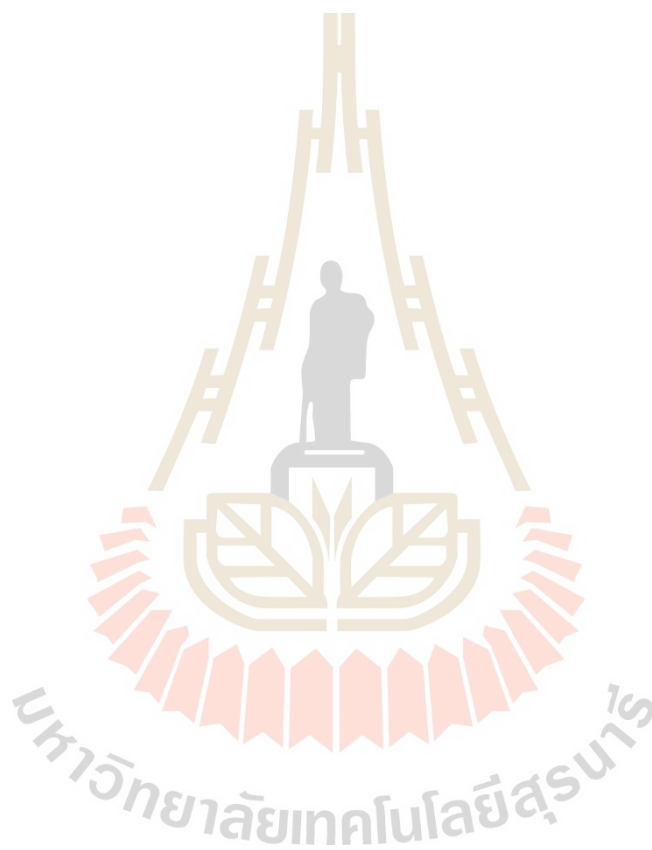
Strunk, J., Vining, W. C. and Bell, A. T. (2011). Synthesis of Different CeO<sub>2</sub> Structures on Mesoporous Silica and Characterization of Their Reduction Properties. **The Journal of Physical Chemistry C.** 115(10): 4114-4126.

Supamathanon, N., Supronowicz, W., Roessner, F., Wittayakun, J. and Prayoonpokarach, S. (2012). Basic properties of potassium oxide supported on zeolite Y studied by pyrrole-TPD and catalytic conversion of methylbutynol. **Química Nova.** 35(9): 1719-1723.

Treacy, M. M. J. and Higgins J.B. (eds) (2001). Collection of Simulated XRD Powder Patterns for Zeolites (4<sup>th</sup> revised edition). **Commission of the International Zeolite Association.**

Wang, N.-N., Wang, Y., Cheng, H.-F., Tao, Z., Wang, J. and Wu, W.-Z. (2013). Impact of cationic lanthanum species on zeolite Y: an infrared, excess infrared and Raman spectroscopic study. **RSC Advances.** 3(43): 20237-20245.

Wu, Y., Wang, J., Liu, P., Zhang, W., Gu, J. and Wang, X. (2010). Framework-Substituted Lanthanide MCM-22 Zeolite: Synthesis and Characterization. **Journal of the American Chemical Society**. 13: 17989-17991.



## CHAPTER V

### CONCLUSION

Cerium - containing zeolite Y are prepared by 3 different methods of Ce adding including ion exchange, impregnation and incorporation. The samples are designed as Ce-NaY-IE, Ce-NaY-IMP and Ce-NaY-INC, respectively. The ion exchange and impregnation strategies preserved the structure and morphology of parent zeolite Y, while incorporation provided zeolite with low crystallinity and amorphous phase. In addition, Ce in the CeO<sub>2</sub> form is detected in all samples with various distribution in zeolite depending on the Ce-introduced method. All samples exhibited different catalytic activity for MBOH conversion. The acidic-basic active sites of all Ce-NaY catalysts are explained by a variety of products from the test reaction.



## APPENDIX

### ONE POT SYNTHESIS OF ZEOLITE NaY

#### Chemicals

Tetraethyl orthosilicate (98% TEOS, Sigma-Aldrich), anhydrous sodium aluminate ( $\text{NaAlO}_2$ , with 41.383%  $\text{Na}_2\text{O}$ , 58.604%  $\text{Al}_2\text{O}_3$ , Riedel-de Haën<sup>®</sup>), hydrochloric acid (37% HCl, Merck) and sodium hydroxide (97% NaOH, Carlo Erba).

#### One Pot Synthesis of Zeolite NaY by acidic co - hydrolysis route

The zeolite was synthesized with a procedure modified from Wu et al. (2010) and Gu et al. (2013). Initially, the gel composition was  $4.62\text{Na}_2\text{O} : \text{Al}_2\text{O}_3 : 10\text{SiO}_2 : 180\text{H}_2\text{O}$ . First, a mixture of 6.25 g TEOS and 3.00 g DI water was stirred vigorously. Subsequently, 0.24 M HCl was added dropwise for pH = 1 adjusting of co-hydrolysis step and it was called solution A. Then, Solution B was obtained from 0.55 g anhydrous  $\text{NaAlO}_2$  which was added into NaOH solution (1.37 g NaOH pellet and 6.41 g DI water) then the mixture was stirred until it became a clear solution before using. After co-hydrolysis, solution B was slowly dropped into solution A under vigorous stirring. Then, NaY precursor was further stirred for 30 minutes followed by aging at room temperature for 24 hours. Finally, it was transferred into a Teflon-lined autoclave and crystallized at 90°C for 24 hours under a static condition. The zeolite

was separated by centrifugation, washed with DI water until the pH of the washed solution is  $\leq 7$ , and dried at 90°C. The obtained solid is named “AB-NaY”.

For comparing the characteristic of obtained material, conventional NaY by basic media method was prepared.

### **Conventional synthesis of NaY by basic media method**

NaY from this route is synthesized with a method modified from Wittayakun et al. (2008). A seed and feedstock gel are prepared and mixed to obtain fixed batch composition as the first sample. Procedure steps followed through IZA with calculated 2 grams of product. Crystallization process is imitated AB-NaY sample. Finally, obtained solid is dried at 110°C overnight and named “B-NaY”

In addition, commercial zeolite Y with sodium form ( $\text{SiO}_2/\text{Al}_2\text{O}_3 = 5.1$ , Sigma-Aldrich), named “C-NaY”, also is used for characteristics comparison with AB- and B-NaY samples.

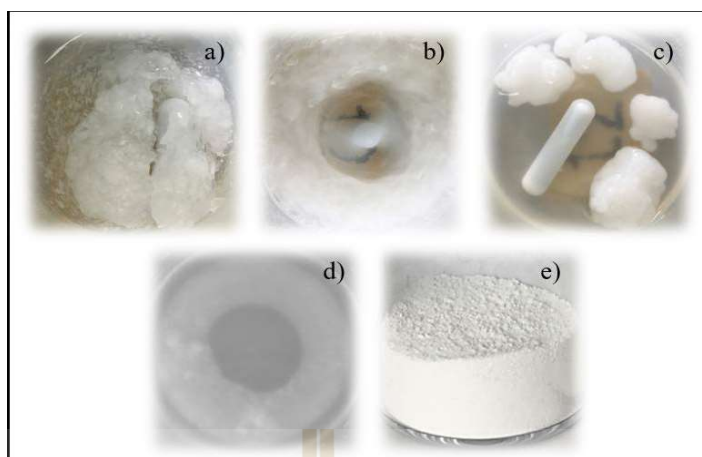
### **Characterization**

Phases of 3 samples are investigated by X-ray diffraction (XRD, Bruker D8 ADVANCE) with a Cu  $K\alpha$  radiation ( $\lambda = 1.5418 \text{ \AA}$ ) operated at voltage and current of 40 kV and 40 mA, respectively. Morphology and crystallinity of all samples are analyzed by scanning electron microscopy (SEM, JEOL JSM-6010 LV and JSM-7800F). Materials vibration bands are studied by Fourier Transform Infrared Spectroscopy (FTIR, Bruker Tensor 27) using Attenuated Total Reflectance (ATR) mode and the spectrum was recorded in the 2000 - 400  $\text{cm}^{-1}$  region. Elementals measurement of Si and Al are determined by using inductively coupled plasma optical

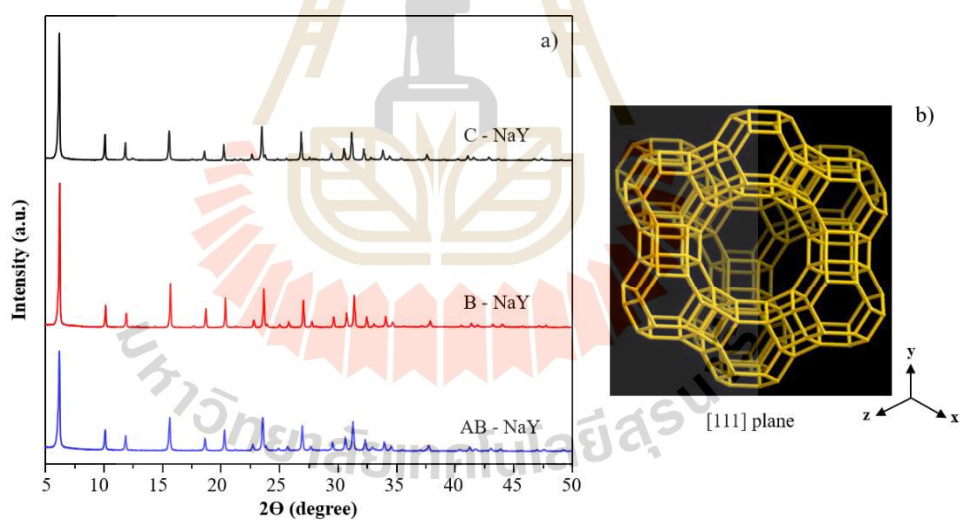
emission spectrometry (ICP-OES, Perkin Elmer Optima 8000). Before quantitative analysis, 50 mg of each sample is digested at 110°C for 1 h by 3.0 mL of 48% HF and 0.5 mL aqua regia of 65% HNO<sub>3</sub> and 37% HCl with the 1:3 volumetric ratio. Then 2.8 g of boric acid and 70 mL of DI water are added to the mixture and shaken to provide clear solution. Afterward, the volume is adjusted to 100 mL in PP volumetric flask. Besides, thermal stability of all obtained materials was evaluated by a thermogravimetric analysis (TGA, Mettler TGA/DSC1). The materials were heated from room temperature to 1,050°C with rate 10°C/1 minute under a flow of nitrogen gas.

## Results and Discussion

Figure 1 reveals the appeared images of AB-NaY one pot synthesis. When Si and Al sources are mixed, it was distinctly seen milky turbid clump (Figure 1a). After keep stirring as in Figure 1b, it gathered and separated into white cluster within clear solution (Figure 1c) which was called non-homogenous precursor. Then crystallization process at 90°C could dissolve almost cluster precursor to like-gel product. Finally, white powder of AB-NaY sample is obtained as in Figure 1(d) and (e).



**Figure 1** Observation images of AB-NaY synthesis; a) after  $\text{NaAlO}_2$  solution was dropped into hydrolyzed TEOS solution, b) while stirring of Si and Al source, c) and d) the mixture before and after crystallization and e) obtained AB-NaY powder.



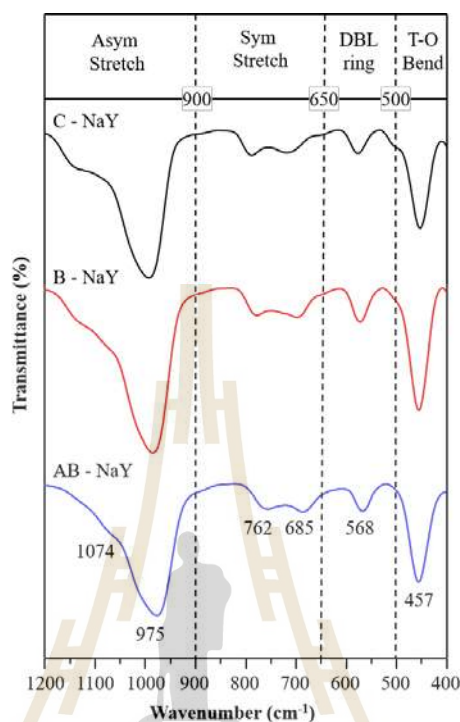
**Figure 2** a) XRD diffraction patterns of zeolite samples and b) faujasite framework viewed along [111] plane.

Figure 2 exhibits XRD analysis of AB-NaY and 2 comparison samples including B-NaY and C-NaY. All diffractograms are similar to faujasite (FAU) structure database from IZA. It characterized from distinct peak at  $2\theta$  around 6.18

degree that represents [111] plane (Figure 2b) of the FAU framework (Mintova and Barrier, 2016). In addition, peaks pattern of AB-NaY preliminary indicates that the non-homogenous precursor from one pot synthesis can provide FAU zeolite with no appearance of other crystallite phases. However, the XRD peak intensity of AB-NaY sample is lower than that of B-NaY, C-NaY. This could attribute from smaller crystal size and/or less crystallinity (Bunmai et al., 2018). From literature, mentioned non-homogenous precursor might be the phenomenon from precipitated amorphous aluminosilicates and/or coagulated silica and alumina precipitated from starting materials destabilized by the change in pH (Cundy et al., 2015). However, over a period of ageing time and heating temperature, equilibration and re-distribution of species between the solid and liquid phases would occur (Cundy et al., 2015). This possibly leads to a final product which is white powder of zeolite.

For further verify the achievable material from one pot synthesis, FTIR spectra in the range of 1200 to 400  $\text{cm}^{-1}$  (Figure 3) are used to illustrate the zeolite characteristic vibrations. The spectra of all samples contain 6 similar observed bands that existed in 4 separated regions (dash lines). Through the spectrum of AB-NaY, the peaks at 457, 685 and 975  $\text{cm}^{-1}$  can be assigned to  $\text{TO}_4$  (T = Si, Al) bending, symmetrical and asymmetrical stretching, serially, of internal tetrahedron linkages. These vibrations can be detected for all aluminosilicates including amorphous zeolite precursors and the primary units of the zeolite (Charkhi et al., 2012 and Lie et al., 2009). While the peaks at 568, 762 and a shoulder at 1074  $\text{cm}^{-1}$  can be attributed to the double ring, symmetrical and asymmetrical stretching, respectively, of external linkages between  $\text{TO}_4$  tetrahedra. The latter 3 bands are observed only when the

zeolitic framework or intertetrahedral O–T–O is constructed which identified by Flanigen, 1976.



**Figure 3** FTIR spectra of all zeolite samples and infrared assignments of 4 characteristic modes vibration and wavenumber positions.

Comparison spectra of B-NaY and C-NaY also contain similar bands of internal tetrahedron and external linkages. However, differences among IR results are clearly seen at the band with shoulder in the region  $900\text{--}1200\text{ cm}^{-1}$ . The band shape and wavenumber position in that region is sensitive to the framework Si/Al ratio. It shifts to a lower frequency with increasing Al content (Miecznikowski and Hanuza, 1985). Hence, from Figure 3, the Si/Al tendency could be approximate as  $\text{C-NaY} > \text{B-NaY} > \text{AB-NaY}$ . This indicates the usefulness of IR to show short-range differences in zeolite structure as opposed to the long-range structure identification ability of XRD.

In addition, the type of one pot zeolite is specified by Si/Al ratio from ICP-OES. The value if Si/Al is 2.49 therefore it can be demonstrated as Y type. The values of B-NaY and C-NaY is 3.55, 3.89, respectively, which consistent with FTIR results.

SEM micrographs of all samples present a similar morphology to zeolite Y from the literatures (Bunmai et al., 2018 and Corso1 et al., 2019) namely, polycrystals with an octahedral shape. It is clearly viewed from the SEM images that B-NaY has higher crystallinity with clear crystal faces and edges than that of AB-NaY and C-NaY samples. This can be attributed from using seed provides synthetic pathway towards a desired phase with reduction of impurities and time (Cundy et al., 2005). Meanwhile, some amorphous particles and/or impurity are observed in AB-NaY images, consistent with crystallinity consideration from XRD intensities. It probably due to non-sufficient crystallization time and/or Si source nature. Mintova and co-workers (1999) studied nucleation mechanism of zeolite Y at 100°C with different time intervals. High-resolution transmission electron microscopy (HR-TEM) results revealed that increasing hydrothermal treatment from 24 to 75 hours transformed amorphous aluminosilicate gel to be well-defined octahedral crystals. They proposed that structural elements at the periphery of the gel phase act as precursors for the nucleation events which mean prolonged time could convert amorphous aggregate into crystalline zeolite Y. Moreover, Oleksiak and Rimer (2014) reported that TEOS or silicate solution is less commonly used in organic structure directing agent (OSDA) - free synthesis of zeolite (in our case is faujasite Y- type). Since, it results in either impurities or non-zeolitic products that likely caused from ethanol occurrence during TEOS hydrolysis.

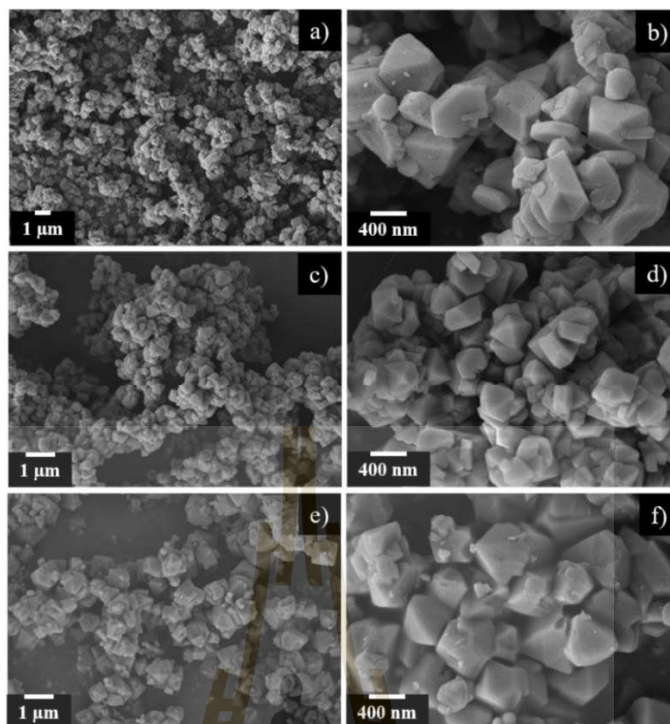


**Figure 4** SEM images of zeolite samples including a, b) C-NaY, c, d) B-NaY and e, f) AB-NaY.

As demonstrated from diffractogram, functional vibration and micrograph results, zeolite NaY could be obtained from our one pot synthesis condition by using TEOS as Si source. This alternative Si precursor also has been studied by Oleksiak and co-workers (Oleksiak et al., 2016). In their case, TEOS was added directly to the mixture of  $\text{NaAlO}_2$  and  $\text{NaOH}$  solution as one pot followed by ageing and hydrothermal treatment. After heating at  $65^\circ\text{C}$  for 168 hours, LTA–FAU binary mixture was obtained from XRD analysis. However, the [111] plane peak of FAU phase was ambiguous. They discussed that since silica from TEOS was slowly hydrolyzed before released into the Al-rich solution, consequently, zeolite nucleation was delayed. Interestingly, when compare to our study, TEOS was firstly hydrolyzed by  $\text{HCl}$  before mixed with  $\text{NaAlO}_2$  solution. It provided XRD pattern of obtained

faujasite Y-type phase with sharp characteristic peak within 24 hours of 90°C heating. Nevertheless, both scenarios cannot be compared straightforwardly since zeolite formation mechanism is not well comprehended. Numerous synthetic parameters and complex processes affect through sequence of induction period, nucleation and crystal growth (Oleksiak et al., 2016).

Thermogravimetric analysis (TGA) of samples are displayed in Figure 5. All thermograms show a weight loss at 80 - 100°C region corresponded to the water desorption. As can be seen, 3 NaY samples are stable until high temperature that normally existed throughout crystalline solid family.

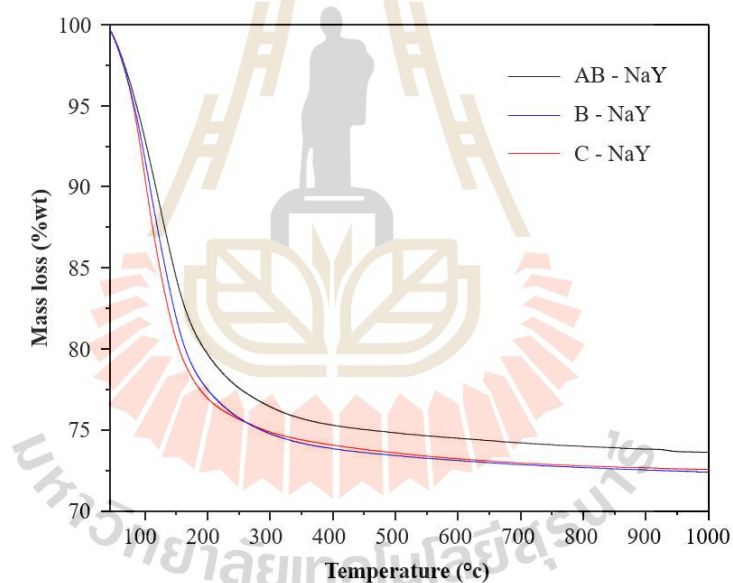


**Figure 5.** TGA thermogram of all zeolite samples.

All of these preliminary characterizations indicate that zeolite NaY formation with high crystallinity and thermal stability is achieved from this one pot experimental design.

## References

- Bunmai, K., Osakoo, N., Deekamwong, K., Rongchapo, W., Keawkumay, C., Chanlek, N., Prayoonpokarach, S. and Wittayakun, J. (2018). Extraction of silica from cogon grass and utilization for synthesis of zeolite NaY by conventional and microwave-assisted hydrothermal methods. **Journal of the Taiwan Institute of Chemical Engineers**. 83: 152-158.
- Charkhi, A., Kazemeini, M., Ahmadi, S. J. and Kazemian, H. (2012). Fabrication of granulated NaY zeolite nanoparticles using a new method and study the adsorption properties. **Powder Technology**. 231: 1-6.
- Cundy, C. S. and Cox, P. A. (2005). The hydrothermal synthesis of zeolites: Precursors, intermediates and reaction mechanism. **Microporous and Mesoporous Materials**. 82: 1-78.
- Corso<sup>1</sup>, C., Silva<sup>1</sup>, M. M., Santana<sup>1</sup>, R. C., Oliveira<sup>1</sup>, K. D. and Ávila-Neto<sup>1</sup>, C. N. (2019) Selection between LTA or FAU phases by manipulating the synthesis gel composition, crystallization time and temperature. **Cerâmica**. 65: 35-44.
- Flanigen, E. M. (1976) Structural analysis by infrared spectroscopy. **ACS Monograph**. 171: 80-117.
- Gu, J., Jin, Y., Zhou, Y., Zhang, M., Wu, Y. and Wang, J. (2013). Unseeded organotemplate-free hydrothermal synthesis of heteroatomic MFI zeolite polynanocrystallites. **Journal of Materials Chemistry A**. 1(7): 2453-2460.
- Khemthonga, P., Klysubunb, W., Prayoonpokaracha, S. and Wittayakun, J. (2010). Reducibility of cobalt species impregnated on NaY and HY zeolites. **Materials Chemistry and Physics**. 121: 131-137.

- Liu, X. (2009). Chapter 5 Infrared and Raman Spectroscopy. Chester, A.W. and Derouane, E.G. (eds.) Zeolite Characterization and Catalysis. **BASF Catalysis Research, R&D Center., New Jersey.**
- Miecznikowski, A. and Hanuza, J. (1985) Application of the long chain approach to the structure and vibrational spectra of X and Y zeolites. **ZEOLITES**. 5: 188-193.
- Mintova, S. and Barrier, N. (Editor) (2016). Verified syntheses of zeolitic materials (2<sup>nd</sup> edition). **Commission of the International Zeolite Association.**
- Oleksiak, M. D. and Rimer, J. D. (2014) Synthesis of zeolites in the absence of organic structure-directing agents: factors governing crystal selection and polymorphism. **Reviews in Chemical Engineering**. 30 (1): 1 - 49.
- Wittayakun, J., Khemthong, P. and Prayoonpokarach, S. (2008). Synthesis and characterization of zeolite NaY from rice husk silica. **Korean Journal of Chemical Engineering**. 25(4): 861-864.
- Wu, Y., Wang, J., Liu, P., Zhang, W., Gu, J. and Wang, X. (2010). Framework-Substituted Lanthanide MCM-22 Zeolite: Synthesis and Characterization. **Journal of the American Chemical Society**. 13: 17989-17991.

# CURRICULUM VITAE

## Wachiraya Rattanawongsa

**Address** 19 No. 29, Khao Sub-district, Maung District, Maha Sarakham,  
Thailand, 44000 Email: Wachiraya.610@gmail.com

### Education

2016

B.Sc. (Chemistry)

Khon Kaen University, Khon Kaen, Thailand

2016 - 2019

Student in M.Sc. program in Chemistry

Suranaree University of Technology, Nakhon Ratchasima,  
Thailand

### Scholarship

2013 - Present

Development and Promotion of Science and Technology  
Talents Project (DPST)